A centronuclear myopathy-causing mutation in dynamin-2 perturbs the actin-dependent structure of dendritic spines leading to excitatory synaptic defects in a murine model of the disease.

Running title: Actin-dependent synaptic defects in dynamin-2-linked CNM

Jorge Arriagada-Diaz[1], Bárbara Gómez[2], Lorena Prado-Vega[1], Michelle Mattar-Araos[3], Marjorie Labraña-Allende[3], Fernando Hinostroza[4], Ivana Gajardo[5], María José Guerra-Fernández[6], Jorge A. Bevilacqua[7], Ana M. Cárdenas[6], Marc Bitoun[8], Alvaro O. Ardiles[6,9,10*], Arlek M. Gonzalez-Jamett[6,11*].

[1]Programa de Magister en Ciencias, Mención Neurociencia, Universidad de Valparaíso, Valparaíso, Chile.
[2] Programa de Magister en Ciencias Médicas, Mención Biología Celular y Molecular, Universidad de Valparaíso, Valparaíso, Chile.
[3] Escuela de Tecnología Médica, Facultad de Medicina, Universidad de Valparaíso, Valparaíso, Chile.
[4] Centro de Investigación de Estudios Avanzados del Maule, CIEAM, Vicerrectoría de Investigación y Postgrado, Universidad Católica del Maule, Talca, Chile
[5] Departamento de Biología Celular y Molecular, Facultad de Ciencias Biológicas, Pontificia Universidad Católica de Chile, Santiago, Chile.
[6]Centro Interdisciplinario de Neurociencia de Valparaíso, Universidad de Valparaíso, Valparaíso, Chile.
[7] Departamento de Neurología y Neurocirugía, Hospital Clínico Universidad de Chile and Departamento de Anatomía y Medicina Legal, Facultad de Medicina, Universidad de Chile, Santiago, Chile.
[8] Sorbonne Université, Inserm, Institut de Myologie, Centre de Recherche en Myologie, F-75013 Paris, France.
[9]Centro de Neurología Traslacional, Facultad de Medicina, Universidad de Valparaíso, Valparaíso, Chile.
[10]Centro Interdisciplinario de Estudios en Salud, Facultad de Medicina, Universidad de Valparaíso, Viña del Mar, Chile
[11] Escuela de Química y Farmacia, Facultad de Química y Farmacia, Universidad de Valparaíso, Valparaíso, Chile.

*correspondence should be addressed to Dr. Arlek M. Gonzalez-Jamett +56-32-2508203 arlek.gonzalez@uv.cl or Dr. Alvaro O. Ardiles +56-32-2507354 alvaro.ardiles@uv.cl

Abstract

Dynamin-2 is a large GTP-ase, member of the dynamin superfamily, that regulates membrane remodeling and cytoskeleton dynamics. In the mammalian nervous system dynamin-2 modulates synaptic vesicle (SV)-recycling at the nerve terminals and receptor-trafficking to and from postsynaptic densities (PSDs). Mutations in dynamin-2 cause autosomal dominant centronuclear myopathy (CNM), a congenital neuromuscular disorder characterized by progressive weakness and atrophy of distal skeletal muscles. Cognitive defects have also been reported in dynamin-2-linked CNM patients suggesting a concomitant impairment of the central nervous system. Here we addressed the mechanisms that lead to cognitive defects in dynamin-2-linked CNM using a knock-in mouse model that harbors the p.R465W mutation in dynamin-2, the most common causing CNM. Our results show that these mice exhibit reduced capability to learn and acquire spatial and recognition memory, impaired long-term potentiation of the excitatory synaptic strength and perturbed dendritic spine morphology, which seem to be associated with actin defects. Together, these data reveal for the first time that structural and functional synaptic defects underlie cognitive defects in the CNM context. In addition our results contribute to the still scarce knowledge about the importance of dynamin-2 at central synapses.

Introduction

Dynamin super-family (DSF) is a group of large GTP-ases that act as mechano-enzymes promoting membrane remodeling in several processes including exocytosis, endocytosis, intracellular trafficking and mitochondrial dynamics among others (Ferguson, et al., 2012; González-Jamett, et al., 2013; Lomash, et al., 2015; Arriagada-Diaz, et al., 2020). Classical dynamins are the best understood members of the DSF. In mammals, these are encoded by three different genes: *DNM1*, *DNM2* and *DNM3* located on chromosomes 9, 19 and 1, respectively (Newman-Smith, et al., 1997; Züchner, et al., 2005; Noakes, et al., 1999). Classical dynamins are composed by five highly conserved domains: an amino-terminal GTP-ase domain that binds and hydrolyze GTP, a middle structural domain, a PH-domain involved in lipid membrane interaction, a GTP-ase effector domain (GED) and an arginine- and proline-rich domain (PRD) that allows dynamin association with SH3-containing proteins (Praefcke, et al., 2004; Ferguson, et al., 2012; Antonny, et al., 2016; Singh, et al., 2017; Arriagada-Diaz, et al., 2020). These domains organize in three regions: a “bundle signaling element” (BSE) composed by helices from the GTP-ase domain and GED, a “stalk” composed by helices from the middle domain and GED, and a membrane-inserting “foot” formed by the PH domain (Chappie, et al., 2009; Faelber, et al., 2011; Ford, et al., 2011; Kong, et al., 2018). In response to the binding of GTP, the BSE convey conformational changes from the GTP-ase domain to the “stalk” promoting dynamin oligomerization in helical structures that enhance its GTP-ase activity and favor membrane scission (Hinshaw, et al., 1995; Warnock, et al., 1997; Antonny, et al., 2016). Dynamin assembly/disassembly cycles and GTP-ase activity also regulate the bundling of the actin cytoskeleton (Gu, et al., 2010; Zhang, et al., 2020; Lin, et al., 2020; Schiffer, et al., 2015a).
The three classical dynamins are expressed at the central nervous system (CNS) and play functions at the pre- and post-synapses (Arriagada-Diaz, et al., 2020). At the pre-synapses they support the endocytic recycling of synaptic vesicles (SVs), exerting differential roles depending on the pattern of neuronal activity (Tanifuji, et al., 2013). In this regard, dynamin-1 mediates SV recycling upon high-frequency stimulation but responding in a slow time window after the arrival of action potentials (APs); dynamin-3 works in a faster time window independent of the frequency of APs and dynamin-2 mediates SV resupply upon high-frequency stimulation with a fast kinetics (Tanifuji, et al., 2013).

At the postsynaptic level dynamin-2 is an important regulator of surface-membrane availability of neurotransmitter-receptors (Carroll, et al., 1999; Kabbani, et al., 2004; Bhatnagar, et al., 2000; Wang, et al., 2017). The latter appears to be especially relevant for glutamatergic excitatory synapses, as dynamin-2 modulate insertion (Jaskolski, et al., 2009), removal (Carroll, et al., 1999; Chowdhury, et al., 2006), and recycling (Lu, et al., 2007; Zheng, et al., 2015) of the α-amino-3-hydroxy-5-methyl-4-isoxazolepropionic acid (AMPA) receptor to and from PSDs.

Although the isoforms -1 and -3 are expressed at a more greater level than dynamin-2 at the CNS (Okamoto, et al., 2001), dynamin-2 seems to play a more critical role for synapse development (Ferguson, et al., 2009). In fact, while embryos of dynamin-1 and/or dynamin-3 knockout (KO) mice survive for weeks after born (Ferguson, et al., 2007; Raimondi, et al., 2011), the KO of dynamin-2 results in early embryonic lethality (Ferguson, et al., 2009).

Mutations in dynamin-2 cause autosomal dominant human diseases (Züchner, et al., 2005; Bitoun, et al., 2005; Tanabe, et al., 2009; Liu, et al., 2011; Koutsopoulos, et al., 2011; Böhm, et al., 2012; Sambuughin, et al., 2015; Ali, et al., 2019). Among them, mutations in the middle and PH domain of dynamin-2 cause the autosomal dominant form of centronuclear myopathy (CNM) a rare neuromuscular disorder clinically manifested by myalgia, fatigability, weakness, and progressive atrophy of distal skeletal muscles (Jeannet, et al., 2004; Fischer, et al., 2006; Böhm, et al., 2012). Cognitive deficiencies, manifested as learning disabilities and limited intelligent quotient, have also been reported in CNM patients (Jeannet, et al., 2004; Fischer, et al., 2006; Echaniz-Laguna, et al., 2007; Böhm, et al., 2012) although the mechanisms involved have never been described. Here we show that a knock-in (KI) mouse model bearing the CNM-causing p.R465W mutation in dynamin-2 (Durieux, et al., 2010; Durieux, et al., 2012) exhibit a deficient capability to learn and acquire spatial and recognition memory. These cognitive defects correlate with impaired hippocampal excitatory synaptic transmission and plasticity. Furthermore, reduced dendritic spine density and changes in spine morphology are also evident in the brain of these mice. This latter seem to rely on defects in the actin cytoskeleton organization. As the catalytic activity of dynamin-2 is an important regulator of the actin dynamics (Mooren, et al., 2009; Gu, et al., 2010; Yamada, et al., 2013; Yamada, et al., 2016; Lin, et al., 2020) and this is a mechanism affected in dynamin-2 linked CNM (González-Jamett, et al., 2017) these data strongly suggest that CNM-causing mutations perturb the synaptic role of dynamin-2, impacting on the actin-dependent dendritic-spine structure and consequently affecting synaptic transmission and cognitive functions.

Results

Impaired learning and memory in adult CNM-mice

As early learning disabilities and cognitive defects have been reported in dynamin-2-related CNM patients (Jeannet, et al., 2004; Fischer, et al., 2006; Echaniz-Laguna, et al., 2007; Böhm, et al., 2012) we first evaluated learning and memory in a murine model of CNM. This is a knock-in mouse harboring the p.R465W mutation located in the middle domain of dynamin-2, the most common mutation causing CNM (Durieux, et al., 2010; Durieux, et al., 2012). Heterozygous mice (HTZ) recapitulate most of the signs of the myopathy, starting at 1 month old (m.o) and progressing as the animal ages (Durieux, et al., 2010). In order to assay learning and memory capabilities, adult HTZ mice over 6 m.o and their age-matched wild type (WT) littermates were subjected to two different behavioral paradigms: the novel object recognition test (NOR) and the Barnes maze (BM). Whilst NOR is useful to evaluate recognition

memory (Ennaceur, et al., 1988), BM is used to measure the ability of mice to learn and remember a spatial location (Rizzo, et al., 2017; Negrón-Oyarzo, et al., 2015; Pitts, et al., 2018).

First, we performed the NOR test. A schematic representation of the test is shown in Figure 1a. As expected WT mice spent significantly more time exploring a novel object (N) than a familial object (F) along sessions (Figure 1b). However HTZ mice did not modify their preference between N and F (Figure 1b) suggesting defects in the recognition memory. Moreover, HTZ mice exhibited a significantly reduced recognition index (D1) compared to their WT littermates (Figure 1c) strongly suggesting a decline in the recognition memory in the CNM context.

Then we applied the BM test. A schematic representation of the test is shown in Figure 1d. WT and HTZ mice were trained during 4 days (training) to find and enter into a hidden scape box using spatial clues. On the fifth day a reversal phase started in which the position of the scape-box was changed but the visual clues were kept to evaluate memory flexibility. As shown in Figure 1e the latency to find and enter into the scape box was decreasing throughout the training sessions for both WT and HTZ mice. However, HTZ mice took a longer time than WT to access the scape box throughout the reversal phase (Figure 1f). In fact, on the last day of the reversal phase WT mice took on average 57.3 ± 18.2 s whereas, HTZ mice took 100.6 ± 20.5 s to end the test (Figure 1f). Remarkably the percentage of HTZ mice that completed the test at the last day of the reversal phase was significantly lower than WT mice (Figure 1g) suggesting defects in spatial memory flexibility. Importantly, these observations did not appear to be due to locomotion defects in HTZ mice as walking time percentage (Figure supplement S1a) and total distance traveled in an open-field arena (Figure supplement S1b) were not different between groups.

Together these data show that the DNM2-linked CNM mouse model shares cognitive impairment with CNM patients and represents a pertinent model to identify the underlying molecular mechanisms

Excitatory synaptic transmission and plasticity are defective in adult hippocampal slices from CNM-mice

Changes in neuronal activity induce modifications in the efficacy of the synaptic transmission; this is known as synaptic plasticity and the mechanisms regulating it are the basis of learning and memory (Shors, et al., 1997). As synaptic plasticity in the hippocampus is particularly important for memory formation (Lee, et al., 2011) and the most studied forms of synaptic plasticity are long-term potentiation (LTP) and long-term depression (LTD) of the synaptic strength at the CA3-to-CA1 synapses (Malenka, et al., 2004) we evaluated excitatory synaptic transmission and plasticity in hippocampal slices isolated from HTZ mice over 6 m.o and their age-matched WT littermates.

The strength of the basal excitatory synaptic transmission was estimated as the I/O relationship. Figure 2a schematizes the experimental configuration for electrophysiological field recordings in hippocampal slices. Figure 2b show representative I/O traces for WT and HTZ hippocampal slices. As shown in Figure 2c the I/O relationship was significantly impaired in HTZ compared to WT slices. HTZ slices exhibited significantly lower fEPSP slopes (Figure 2d) but significantly higher FV-amplitudes (Figure 2e) compared to the WT condition. To evaluate whether plasticity of the synaptic strength is also affected in the CNM-context we induced NMDAR-dependent LTP in WT and HTZ hippocampal slices by using a standard theta

burst stimulation (TBS) protocol that drives a compound-LTP, involving pre- and post-synaptic mechanisms (Bayazitov, et al., 2007). Whilst LTP induction relies on the activation of NMDAR- that requires both presynaptic glutamate release and post-synaptic depolarization (Citri, et al., 2008), LTP maintenance mainly relies on AMPAR trafficking at the PSDs (Anggono, et al., 2012a). As shown in Figure 3 the magnitude of the TBS-induced LTP was significantly reduced after 50 min of record in HTZ compared to WT hippocampal slices (Figures 3a and 3c) suggesting a role of dynamin-2 in the maintenance of the tetanus-induced LTP. Furthermore, the early potentiation of the synaptic response measured during the first 5 minutes after the application of TBS was also reduced in HTZ compared to WT slices (Figure 3b) suggesting that LTP-induction is also dependent on dynamin-2. To evaluate the presynaptic contribution to the defects observed in HTZ synapses we estimated a paired-pulse facilitation (PPF) index (Figure 3d-e). PPF is a form of short-term synaptic plasticity that occurs when two stimulation-pulses of similar intensities are given in rapid succession, causing the second synaptic response to be bigger than the first one (Zucker, et al., 2002). Facilitation appears to be due to an increased presynaptic Ca^{2+} concentration that leads to enhanced neurotransmitter-release probability (Zucker, et al., 2002). The PPF index was unchanged between HTZ and WT hippocampal slices (Figure 3d-e) suggesting that, although presynaptic mechanisms could operate in the CNM-context, those appear to be independent of the release probability. Hence, the p.R465W mutation in dynamin-2 seems to mainly affect post-synaptic mechanisms, impairing synaptic potentiation upon sustained neuronal activity. The main post-synaptic impact was confirmed by a chemically induced LTP using the NMDAR-agonist Glycine (chLTP) which activates NMDAR without mediating a presynaptic glutamate release (Lu, et al., 2001; Zhang, et al., 2014). Upon chLTP a significant reduction in the magnitude of synaptic potentiation was observed in HTZ compared to WT slices (Figure supplement S2). Interestingly, these postsynaptic mechanisms appear to predominantly affect excitatory synaptic transmission, as we observed similar differences between HTZ and WT slices when the TBS protocol was elicited in the presence of *picrotoxin* (*PTX*), a blocker of the GABAR-dependent inhibitory transmission (Figure supplement S3).

Like LTP, LTD is a relevant long-term synaptic plasticity phenomena also implicated in learning and memory (Malenka, et al., 2004; Citri, et al., 2008). We evaluated weather LTD is also affected in the CNM-context and observed a significant reduction in the LTD-magnitude in HTZ compared to WT slices (Figure supplement S4).

Altogether these data demonstrate that the excitatory synaptic transmission and plasticity are DNM2-dependent processes impaired in the CNM context.

Dendritic-spine morphology is perturbed in neurons from adult CNM-mice

Besides a functional excitatory synaptic plasticity that mainly relies on changes in AMPAR activity at the PSDs (Anggono, et al., 2012b) there is a structural plasticity involving morphological changes at dendritic spines. Dendritic spines are actin-enriched protrusions where occur most of the excitatory synapses (Bosch, et al., 2012). Their density, size and shape correlate with the degree of synapse maturity and functionality and undergo modifications upon synaptic plasticity. In this regard it has been demonstrated that LTP-induction increases dendritic spine density and promotes the transit towards a

202 mature-spine shape with higher head diameter leading to a higher head/spine length ratio (Matsuzaki,
203 et al., 2001; Okamoto, et al., 2009). On the contrary, LTD-induction reduces dendritic spine density and
204 leads to the shrinkage of pre-existing spines (Okamoto, et al., 2004). In order to evaluate whether the
205 defects in excitatory synaptic transmission and plasticity observed in HTZ slices were related to
206 structural defects in dendritic spines, we marked brains from 6 m.o WT and HTZ mice with a Golgi- -
207 staining and quantified dendritic spine density and morphology in hippocampal and cortical neurons.
208 Figures 4 and 5 summarize observations made on hippocampal and cortical pyramidal neurons,
209 respectively. The comparison of the mean morphological parameters revealed a significant reduction in
210 spine density (number of spines per 1 µm of dendritic shaft) in HTZ compared to WT hippocampal
211 neurons (Figure 4b). Although no significant differences were observed in the spine shape on average
212 (Figure 4c) HTZ hippocampal neurons tended to exhibit a lower percentage of filopodial-protrusions and
213 a higher percentage of stubby-like spines. To further evaluate dendritic spine structure, we quantified
214 the cumulative frequency of spine lengths, head diameters and head/length ratios. Remarkably,
215 although head diameters were not different between WT and HTZ hippocampal neurons (Figure 4d)
216 these latter exhibited a significantly higher frequency of shorter spines, producing a leftward shift in the
217 cumulative distribution curve compared to WT spines (Figure 4e). As a consequence of having shorter
218 dendritic spines, HTZ hippocampal neurons also exhibited a significantly higher head diameter/spine
219 length ratio compared to WT neurons (Figure 4f).
220 Similar to that observed in hippocampal neurons, HTZ cortical neurons exhibited a significantly lower
221 mean spine density (Figure 5b) and tended to show a lower proportion of filopodial-protrusions
222 compared to the WT condition (Figure 5c). Remarkably, cortical HTZ neurons exhibited a higher
223 frequency of spines with smaller heads (Figure 5d) and shorter lengths (Figure 5e) although the
224 head/length ratio was unchanged (Figure 5f).
225 Together, these data suggest that pyramidal neurons bearing the dynamin-2 p.R465W mutation may
226 undergo modifications in density, head width and length of dendritic spines.

227 ***Impaired F-actin organization in CNM-neurons***

228 As dendritic spine morphology critically depends on the underlying actin network (Okamoto, et al.,
229 2009; Hotulainen, et al., 2010; Matus, et al., 2000) and actin dynamics is significantly affected in the
230 CNM context (González-Jamett, et al., 2017) we next evaluated actin organization in brains of WT and
231 HTZ mice. Relative amounts of filamentous (F-) and monomeric (G-) actin were quantified in the
232 hippocampus and cortex. Figure 6 shows representative blots from hippocampal (Figure 6a) and cortical
233 tissues (Figure 6b) and the quantification of the respective F/G ratios. Our results indicated that the
234 balance between F- and G-actin is perturbed in brains of HTZ compared to WT mice. Specifically the F/G
235 ratio increased from 1.9 ± 0.5 to 3.9 ± 1.3 in HTZ compared to WT hippocampal tissue (Figure 6a). In the
236 cortex the F/G ratio increased from 0.6 ± 0.01 to 2.1 ±0.8 in HTZ compared to WT brains (Figure 6b).
237 These data suggest that the modifications in dendritic spine morphology experienced by HTZ neurons
238 (Figures 4-5) could rely on actin cytoskeleton disturbances in adult mice. To further explore this
239 possibility early in the disease development, we evaluated dendritic spine morphology in hippocampal
240 neurons from WT and HTZ neonates (P0). 7 days *in vitro* (7*DIV*) neuron primary cultures were fixed,
241 stained with the F-actin-binding toxin phalloidin-rhodamine-B and visualized by confocal microscopy.
242 Unlike what we observed in neurons from adult mice (Figures 4-5), the mean density of spines stained
243 with phalloidin was not different between neonate-derived WT and HTZ neurons (Figure 7b). However
244 HTZ neurons tended to exhibit a higher percentage of filopodial protrusions and a lower proportion of
245 stubby-like spines compared to WT neurons (Figure 7c) suggesting that the actin-dependent spine
246 development is delayed in HTZ neurons. It is noteworthy that we were not able to observe branched
247 mature spines in cultured neurons. We also quantified the cumulative frequency of spine head

diameter, spine length and head/length ratio. Although head diameters of phalloidin stained-spines were not different between WT and HTZ neurons (Figure 7d), HTZ neurons exhibited a significantly higher frequency of longer spines (Figure 7e) and lower head/spine ratios compared to WT neurons (Figure 7f). This latter supports the idea that actin-dependent dendritic spine features could be early impaired in the CNM context. In this regard, the phalloidin-fluorescence intensity was significantly lower in HTZ compared to WT spines (Figure supplement S5) suggesting that the F-actin network underlying HTZ spines is impaired.

All together the results presented here demonstrate that dynamin-2 is an important regulator of the excitatory synaptic transmission in the mammalian brain, by modulating actin-dependent dendritic spine structure. This dynamin-2 function appears to be perturbed by the p.R465W mutation, impairing synaptic structure and function and consequently leading to cognitive defects in the CNM context.

Discussion

Dynamin-2 is a large GTP-ase, member of the dynamin superfamily, that regulates membrane remodeling and actin dynamics, orchestrating actin and membrane-based processes such as exocytosis (González-Jamett, et al., 2013; Shin, et al., 2018), endocytosis (Van der Bliek, et al., 1993; Damke, et al., 1994; Loerke, et al., 2009) and endosomal recycling (Nicoziani, et al., 2000) among others.

In the nervous system, dynamin-2 is expressed at the pre-and post-synaptic levels (Okamoto, et al., 2001). At the pre-synapses dynamin-2 participates in the endocytic recycling of SVs, allowing the resupply of the ready-releasable pool in response to high frequency neuronal activity (Tanifuji, et al., 2013). At the post-synapses dynamin-2 regulates the availability of neurotransmitter receptors at the surface membranes (Carroll, et al., 1999; Kabbani, et al., 2004; Bhatnagar, et al., 2001; Wang, et al., 2017). Of particular relevance for excitatory synaptic transmission is the role played by dynamin-2 in AMPAR trafficking. The GTP-ase activity of dynamin-2 is required for the insertion of AMPAR into spines, by mediating their lateral diffusion from dendritic shafts to PSDs (Jaskolski, et al., 2009). In addition, dynamin-2 GTP-ase activity has been implicated in the removal (Carroll, et al., 1999; Chowdhury, et al., 2006) and recycling (Lu, et al., 2007; Zheng, et al., 2015) of AMPARs from and to PSDs. Hence, as AMPAR mediates the majority of fast excitatory synaptic transmission in the mammalian brain (Anggono, et al., 2012a), dynamin-2 could play a key regulatory function, supporting synaptic transmission and plasticity. In agreement with this idea, pharmacological inhibition of dynamin´s GTP-ase activity with dynole 34-2 (Arriagada-Diaz, et al., 2020) or dynasore (Fa, et al., 2014) significantly reduces LTP in hippocampal slices. Here, we demonstrate that the CNM-causing p.R465W mutation negatively impacts on the synaptic function of dynamin-2, leading to defects in excitatory synaptic transmission and plasticity in the brain of HTZ mice. As dynamin-2 is mostly expressed at the post-synaptic level (Okamoto, et al., 2001) it is likely that these HTZ defects in synaptic transmission rely on post-synaptic mechanisms such as AMPAR trafficking. Indeed, we observed a reduction in the magnitude of LTP in HTZ slices when we induced potentiation both electrically as well as when we did it chemically with glycine. As the chLTP protocol elicits potentiation of the synaptic strength by directly activating NMDARs without mediating the presynaptic release of glutamate (Lu, et al., 2001; Zhang, et al., 2014), these results are consistent with major post-synaptic mechanisms underlying HTZ synaptic defects. In fact, the PPF index was unchanged between WT and HTZ hippocampal slices (Figure 3d). As PPF is an estimation of the neurotransmitter release probability (Zucker, et al., 2002) it is unlikely that the changes that we observed in excitatory synaptic transmission in HTZ hippocampal slices are related to changes in the glutamate release probability. This is agreement with a recent report of Moro and collaborators who found that dynamins are dispensable for synaptic vesicle exocytosis (Moro, et al., 2021).However, we cannot rule out presynaptic defects in the CNM context. The fact that the amplitude of the fiber volley was significantly higher in HTZ compared to WT slices (Figure 2) could mean that more presynaptic

295 terminals are recruited in order to compensate a reduction in the SV releasable pool. As dynamins´s
296 GTP-ase activity of dynamin-2 regulates SV recycling (Tanifuji, et al., 2013; Watanabe, et al., 2013;
297 Cheung, et al., 2019) it is possible to visualize a scenario in which the p.R465W mutation in dynamin-2
298 affects the size of the SV releasable pool, impacting neurotransmission. More experiments are needed
299 to address this possibility.
300 Regardless of whether defects were pre or post-synaptic, there was a significant impairment in synaptic
301 transmission and plasticity in HTZ compared to WT brains. Congruently, HTZ mice exhibit a cognitive
302 decline, manifested as defects in recognition and spatial memory which can be explained by
303 perturbations in the synaptic function. In this regard, even though CNM primarily affects skeletal
304 muscles (Romero, et al., 2011; González-Jamett, et al., 2017) learning disabilities and limited intelligent
305 quotient have been reported in dynamin-2-linked CNM patients (Jeannet, et al., 2004; Fischer, et al.,
306 2006; Echaniz-Laguna, et al., 2007; Böhm, et al., 2012). As we observed here in HTZ mice, cognitive
307 defects manifested by CNM patients could be due to disturbances in the synaptic function. Remarkably,
308 in addition to changes in the synaptic strength, we also observed structural modifications in dendritic
309 spines of the HTZ compared to WT neurons. In this regard, dendritic spine density was significantly
310 lower in pyramidal neurons from adult HTZ mice (Figures 4-5). As the majority of the synaptic contacts
311 between excitatory neurons are made on dendritic spines (Harris, et al., 1994) a net reduction in spine
312 density can lead to significant defects in synaptic transmission, such as those observed in HTZ
313 hippocampal slices. Moreover, dendritic spine morphology, which is closely related to the maturity and
314 functionality of synapses (Holtmaat, et al., 2009; Gipson, et al., 2017), also underwent modifications in
315 HTZ compared to WT neurons (Figures 4, 5 and 7). Although on average we did not observe significant
316 differences in spine morphology between genotypes, the cumulative distribution of the spine length,
317 spine head diameter and head/length ratio yielded important variations. Whilst mature HTZ
318 hippocampal neurons exhibited a higher frequency of shorter spines, neonatal hippocampal neurons
319 cultured from HTZ pups showed a higher frequency of immature larger spines with a significant
320 reduction in the head diameter/spine length ratio. Moreover, cortical neurons from adult HTZ brains
321 exhibited higher frequency of shorter spines, with smaller heads compared to WT neurons. As spines
322 with large head and large head/spine ratio have been found to correlate with an increased PSD area and
323 AMPAR density (Matsuzaki, et al., 2001) a reduction in spine head diameter or the head/length ratio
324 could explain defects in synaptic transmission and plasticity.
325 A major factor regulating spine morphology is the actin cytoskeleton (Okamoto, et al., 2004; Bosch, et al., 2014). A
326 dynamic F-actin network exists in dendritic spines which act primarily as a cytoskeleton component defining spine
327 architecture, but also as a scaffold for the recruitment of post-synaptic proteins including AMPAR (Okamoto, et al.,
328 2009; Cingolani, et al., 2008; Stefen, et al., 2016).Therefore, remodeling of spine-actin is critical for structural and
329 functional synaptic plasticity (Kim, et al., 1999; Okamoto, et al., 2004) and it is not surprising that perturbations in
330 actin dynamics lead to different synaptopathies (Penzes, et al., 2012; Pelucchi, et al., 2020). Thus, the changes that
331 we observed in the density and shape of dendritic spines in HTZ neurons are compatible with defects in actin
332 dynamics. Indeed, we previously demonstrated that actin organization and remodeling are disrupted in muscle
333 cells of HTZ mice (González-Jamett, et al., 2017) and our results here suggest an imbalance between F- and G-actin
334 in the hippocampus and cortex of adult HTZ mice. The fact that the observed differences did not reach statistical
335 significance when compared total brain homogenates (Figure 6) could be due to the F/G imbalance is more
336 important in neurons than in other cell types. If that is true such differences may be attenuated in total
337 homogenates in which more of the cells are glia. An increase in the F/G ratio as we observed in HTZ compared to
338 WT brains (Figure 6) could be related to a less dynamic neuronal actin network, with a reduced ability to remodel
339 itself to support synaptic transmission. In the case of neonatal cultured neurons, the fluorescence intensity of the
340 F-actin-binding toxin phalloidin at the dendritic spines was significantly lower in the HTZ compared to WT condition
341 (Figure supplement S5). This latter strongly suggests that the F-actin network that supports dendritic spine
342 structure is perturbed in HTZ neurons. But, how the p.R465W mutation could impact on dynamin-2 function
343 leading to defects in actin and actin-based mechanisms? The residue 465 localizes near to a putative direct actin-
344 binding motif in dynamin-2 (Gu, et al., 2010, red region in Figure 8a). As these authors proposed, unassembled

345 dynamins could bind to short actin filaments via their middle domain and in turn oligomerize in rings promoting
346 actin polymerization (Gu, et al., 2010; Gu, et al., 2014; Shiffer, et al., 2015). If that is true, the substitution of a
347 positive-charged arginine by a non-polar tryptophan in the oligomerization-middle domain of dynamin-2 could
348 certainly influence its actin-binding properties affecting actin dynamics. In this regard, by using full-atom and
349 coarse-grained molecular simulations, we previously demonstrated that the p.R465W mutation affects the
350 interaction between the residue 465 and surrounding amino acids, modifying the conformation of the BSE and
351 consequently impacting on the GTPase-domain position and dynamin-2 self-assembly (Hinostroza, et al., 2020).
352 Recent evidences suggest that helix of dynamin-2 interact with F-actin via their outer-rim (Zhang, et al., 2020). This
353 region includes the C-terminus PRD that is adjacent to the GTPase domain and to the BSE (Figure 8b). It is
354 noteworthy that the R/W 465 residue interacts with the BSE in a region that is close to the starting point of the
355 PRD (Figures 8b-c). As the p.R465W mutation in dynamin-2 extends the angle between the G domain and the BSE
356 (Hinostroza, et al., 2020) in the tetramer and helical configuration (Figure 8d) we speculate that the
357 arginine/tryptophan substitution in the residue 465 not only modifies the BSE conformation but also changes the
358 position of the PRD, being able to affect the PRD-actin interaction. This assumption is in agreement with a model in
359 which the actin-remodeling activity of dynamin-2 is disrupted by CNM-causing mutations. In accordance with this
360 idea, Lin and collaborators recently demonstrated that dynamin-2 regulates the bundling of actin at the
361 postsynaptic membranes of neuromuscular junctions (NMJs). Remarkably, CNM-linked mutations seem to disrupt
362 this dynamin-2 function impairing actin remodeling and perturbing postsynaptic structures at the NMJs (Lin, et al.,
363 2020). A similar mechanism could be operating at central excitatory synapses in the brain of HTZ mice, explaining
364 the defects that we observed in dendritic spine morphology, synaptic transmission and cognitive functions.

365 In our knowledge, this is the first report addressing the mechanisms that lead to cognitive defects in dynamin-2-
366 linked CNM. Our data support a model in which the actin cytoskeleton organization is impaired, leading to
367 structural and functional synaptic defects. In addition, our results contribute to the better understanding of the
368 still scarce knowledge about the function of dynamin-2 at central synapses.

369

370 **Methods**

371 *Animals*
372 HTZ mice harboring the p.R465W mutation in dynamin-2 is a mammalian model of CNM. These mice
373 recapitulate most of the CNM-signs, which start at 1 mo and progress as animals age (Durieux et al.,
374 2010). HTZ and WT littermates (C57BL/6 strain) were housed at room temperature with *ad libitum*
375 access to food and water. Mice were maintained on light-darkness cycles of 12–12 h, according to
376 standard protocols. Genotyping was performed by PCR as previously described (Durieux et al., 2010)
377 using DNA extracted from ears. Primers used were: 3'-CTGCGAGAGGAGACCGAGC-5' (forward) and 3'-
378 GCTGAGCACTGGAGAGTGTATGG-5 (reverse). PCR products were electrophorated in agarose gels and
379 bands of 445 bp and 533 bp, representing the WT and p.R465W mutated allele respectively, were
380 detected. All animal protocols described here were conducted in accordance with the approved
381 protocols of the Institutional committee for the care of laboratory animals of Universidad de Valparaíso
382 (BEA131-18).
383
384
385
386 *Behavioral tests*
387 Recognition and spatial learning and memory were assessed in 6 m.o WT and HTZ mice by application of
388 the Novel Object Recognition (NOR) test and the Barnes maze test (BM), respectively. Locomotion
389 capabilities in mice were evaluated by application of a standard Open Field (OF) test. All behavioral

390 tests were carried out in a room conditioned for this purpose, with controlled temperature (21 ° ± 2 ° C),
391 white noise (50 dB) and regulated luminosity (200 lux).
392
393 *NOR.* This test is based on the spontaneous tendency of rodents to spend more time exploring a novel
394 object than a familial one. Maze consisted of a 50 cm x 40 cm x 63 cm square white acrylic box in which
395 mice explored freely during 5 min throughout three phases: (i) sample, where mice explored a pair of
396 identical objects; (ii) retention, where mice were removed for cleaning and changing objects; and (iii)
397 choice, where mice explored a pair of different objects: a familiar object (F) and a new object (N). Each
398 session was repeated during 3 days. The time that mice spent exploring F or N was quantified. A
399 recognition index (D1) was calculated as [N exploration time-F exploration time.
400 *BM*. This task is dependent on the intrinsic inclination of rodents to escape from an aversive
401 environment (Barnes 1979). It consists in a 70 cm diameter white circular platform elevated 90 cm from
402 the floor with 20 equally spaced holes along the perimeter (each 7 cm in diameter) located 2 cm from
403 the edge of the platform. The animals are oriented by means of spatial clues located on the walls of the
404 room, in order to find and remember the position of a black plexiglass escape box (17 × 13 × 7 cm) that
405 is hidden under one of the holes. The maze was illuminated with 4 incandescent lights to produce a light
406 level of around 600 lux fall on the circular platform. BM test consisted of 9 session days, 4 trials per
407 session along which three phases were carried out: (i) pre-training phase, where mice were trained to
408 find the escape platform (ii) training phase, where mice remember the position of the escape box
409 guided by the spatial clues arranged in the room, (iii) reversion phase, where the location of the escape
410 box was changed but maintaining the position of the spatial clues to evaluate memory flexibility. In all
411 phases, if mice did not find the target hole and did not enter into the escape box during 3 minutes, the
412 test was terminated. Subsequently, the experimenter guided the animal to the escape box and allowed
413 it to remain in the box for 1 minute before returning to their holding box. Latency or time that took to
414 animals to find the target hole and enter into the scape box was quantified.
415 *OF.* Mice were placed in the center of a 50 cm x 40 cm x 63 cm white acrylic box and left to explore
416 freely during 5 minutes, along 3 sessions (1 session per day). Total distance traveled and the percentage
417 of walking time was quantified.
418
419 *Field electrophysiological recordings*
420 To evaluate basal strength of synaptic transmission and synaptic plasticity we evoked field excitatory
421 postsynaptic potentials (fEPSPs) in WT and HTZ hippocampal slices by stimulating the Schaffer
422 Collaterals (CA3) and recording the synaptic responses in *stratum radiatum* of CA1. Hippocampal slices
423 were prepared as previously described (Ardiles et al. 2014). Animals were euthanized under deep
424 anesthesia using isoflurane at saturation and their brains were quickly removed after craniotomy. Brains
425 were sectioned in two hemispheres, removing hippocampus to be sectioned in 300 µm thick slices and
426 immersed in dissection buffer (in mM: 212.7, sucrose 26 $NaHCO_3$, 1.23 NaH_2PO_4, 10 D-glucose, 5 KCl, 2
427 $CaCl_2$, 1 MgCl, 3 pyruvate) using vibratome (Vibratome 1000 plus, Ted Pella Inc., CA, USA). Slices were
428 transferred and kept for 1 hour at room temperature in artificial cerebrospinal fluid (ACSF, in mM: 124
429 NaCl, 26 $NaHCO_3$, 1.23 NaH_2PO_4, 10 D-glucose, 5 KCl, 2 $CaCl_2$, 1 MgCl, 3 pyruvate). All recordings were
430 obtained in an immersion chamber perfused with ACSF (30 ± 0.5°C; 2 ml / min). Stimulation was
431 performed with pulses of 0.2 ms duration, administered through concentric bipolar stimulation
432 electrodes. Basal responses were recorded using mean stimulation intensity compared to maximum.
433 Basal synaptic transmission was analyzed by determining input-output relationship (I /O) of the fEPSP

434 generated by gradually increasing the stimulation intensity. Input corresponded to the amplitude of the
435 fiber volley and the output to the initial slope of the fEPSP. To evaluate long-term potentiation (LTP),
436 slices were subjected to a high-frequency electrical stimulation protocol or a chemical stimulation
437 protocol. LTP using high-frequency electrical stimulation was performed using a standard theta burst
438 (TBS) protocol, which consists of 4 trains at 100 Hz for 1 min (Flores-Muñoz et al. 2020; Gajardo et al.
439 2018). On the other hand, chemical LTP (chLTP) was induced by perfusing a glycine solution (glycine, Gly
440 600 µM + *picrotoxin*, PTX 50 µM + strychnine Stric 3 µM) (X. Y. Zhang et al. 2014), directly on the
441 hippocampal slices during 5 minutes. Gly is co-agonist of NMDAR, PTX is an inhibitor of the inhibitory
442 GABAR-dependent transmission and Stric is an inhibitor of Gly-receptors. Once the application time of
443 solution had elapsed, it was removed and the registration buffer was replaced with a new one. In both
444 cases, fEPSPs were recorded for 20 minutes prior to stimulation and for 50 minutes after the application
445 of the electrical stimulus (TBS) or chLTP.
446 To assess long-term depression (LTD), a standard low-frequency electrical protocol was induced which
447 consists of a 1 Hz stimulation for 15 minutes (Gajardo et al. 2018). fEPSPs were recorded for 20 minutes
448 prior to stimulation and for 60 minutes after the application of LFS.
449 Paired pulse facilitation (PPF) was obtained by stimulating at different intervals in a range between 25-
450 300 ms and recording excitatory post-synaptic potential (EPSP). A PPF index was estimated by dividing
451 the amplitude of the second response over the first one (R2/R1).
452
453 *Spine density and morphology*
454 HTZ mice over 6 mo and age-matched WT littermates were sacrificed, brains were quickly removed and
455 processed using the FD Rapid Golgi-Stain-TM kit (FD Neuro Technologies) according to the manufacturer
456 instructions. Golgi impregnated cortical and hippocampal neurons were imaged using a Leica DM500
457 microscope equipped with a camera system, a 63X /1.40 oil (HCPL Apo, Leica) objective and the Leica
458 acquisition software. Pyramidal neurons were analyzed and processed using the ImageJ software (NIH,
459 USA). To evaluate the spine density and morphology, measurements were performed in dendritic
460 segments of 10 to 20 µm, visualized from four apical dendrites per neuron. Dendritic- protrusions were
461 categorized following the parameters revised by Risher and collaborators (Risher et al., 2014). Long, thin
462 without-head protrusions of more than 2 um long were classified as immature filopodia; wide-head
463 (>0.6 um width) and short protrusions (<1 um) were classified as mature mushroom-spines; wide-
464 head/without neck protrusions (length: width ratio <1 um) were classified as stubby-spines; thin and
465 short (<2 um) headed protrusions were classified as thin-spines. Cup-shaped protrussions were
466 classified as branched spines (Figure Supplement S6). Measurements were made by two different
467 experimenters, blind to the genotype of the samples.
468
469
470
471 *Neuron primary culture*
472 Hippocampal neurons were primary cultured from post-natal mice (P0) following the protocol described
473 by Beduoain and collaborators (Beduoain et al., 2012). Briefly, hippocampi from individual pups were
474 dissected, trypsinized for neurons dissociation and plated in poly-L-lysine treated coverslips and
475 maintained in medium containing B27-supplement (GIBCO), glutamax (GIBCO) and
476 Penicilin/Streptomycin mixture of antibiotics (GIBCO). Genotype of each single culture was confirmed a
477 *posteriori* from tail-segments of pups. 2 days after culture neurons were treated with 5µM cytosisne-
478 arabinoside (Ara-C) to inhibit the proliferation of non-neuronal cells. At 7 *DIV,* neurons were fixed with

479 4%PFA + 4% sucrose during 10 min at 37°C, permeabilized with 0.1% triton-X100 in saline phosphate
480 buffer (PBS, mM: 137 NaCl, 2.7 KCl, 10 Na_2HPO_4, 2 KH_2PO_4, pH 7.4) during 10 min at room temperature
481 and stained during 1 h with 1µM phalloidin-Rhodamin-B (Sigma) before confocal visualization. Images
482 were acquired in a confocal microscope (upright Eclipse Nikon 80i) using a 60x magnification objective.
483 Single confocal images were acquired with the EZ-C1 (Nikon) software using similar acquisition settings
484 between comparable samples. Analyses of dendritic spines stained with phalloidin were made with the
485 ImageJ software (NIH, USA) by two different experimenters, blind to the genotype of the samples. The
486 phalloidin fluorescence intensity was measured inside spines, without including the neighboring
487 dendritic shaft.
488
489 *F/G actin assay*
490 Hippocampal and cortical tissue from WT and HTZ mice were lysed and homogenized in conditions that
491 stabilize filamentous (F-) and monomeric (G-) actin using an F/G actin commercial assay (Cytoskeleton
492 Inc.). Lysed extracts were ultracentrifuged at 100,000 g for 1 h at 37 °C in order to separate pellets (F-
493 actin) and soluble (G-actin) fractions. The F-actin pellet was resuspended in a depolymerizing buffer
494 (Cytoskeleton Inc) and then F-and G-actin fractions were diluted in loading buffer (50 mM Tris–HCl, 2%
495 SDS, 10% glycerol, 1% beta-mercaptoethanol and bromophenol blue). Samples were subjected to
496 electrophoresis in 12%-SDS-PAGE, transferred to a PVDF membrane, blocked for 1 h with 5% non-fat
497 milk in TBS-T (mM:150 NaCl, 50 Tris/HCl, pH 7.4, 0.05% Tween-20), incubated with a polyclonal antibody
498 against actin (1:500; Cytoskeleton Inc.) and developed by chemiluminescence. Densitometric analysis of
499 the F- and G-actin bands was performed with the ImageJ software.
500
501 *Statistical analyses*
502 GraphPad Prism 9 software was used to perform the statistical analyses. Paired or unpaired non-
503 parametric Mann-Whitney test were used to compare WT and HTZ conditions. Two-way ANOVA
504 followed by Bonferroni multiple comparison post-test was also used in electrophysiological experiments.
505 Data in graphs represent the mean ± SEM, with a p-value <0.05 being significant. If not specified,
506 differences were not statistically significant.
507
508 **Declaration of Conflicting Interests**
509
510 The author(s) declared no potential conflicts of interest with respect to the research, authorship, and/or
511 publication of this article.
512
513 **Acknowledgements**

514 We thank Dr. Isaac García-Carrillo for facilitating facilities for western blot development. This work was
515 supported by the grants Fondecyt 11180731 (to AMG-J), Fondecyt 1201342 (to AOA), and ICM-ANID
516 ICN09-022 CINV (to AMG-J, AOA, and AMCD) and by ANID scholarship 22200154 (to JA-D).

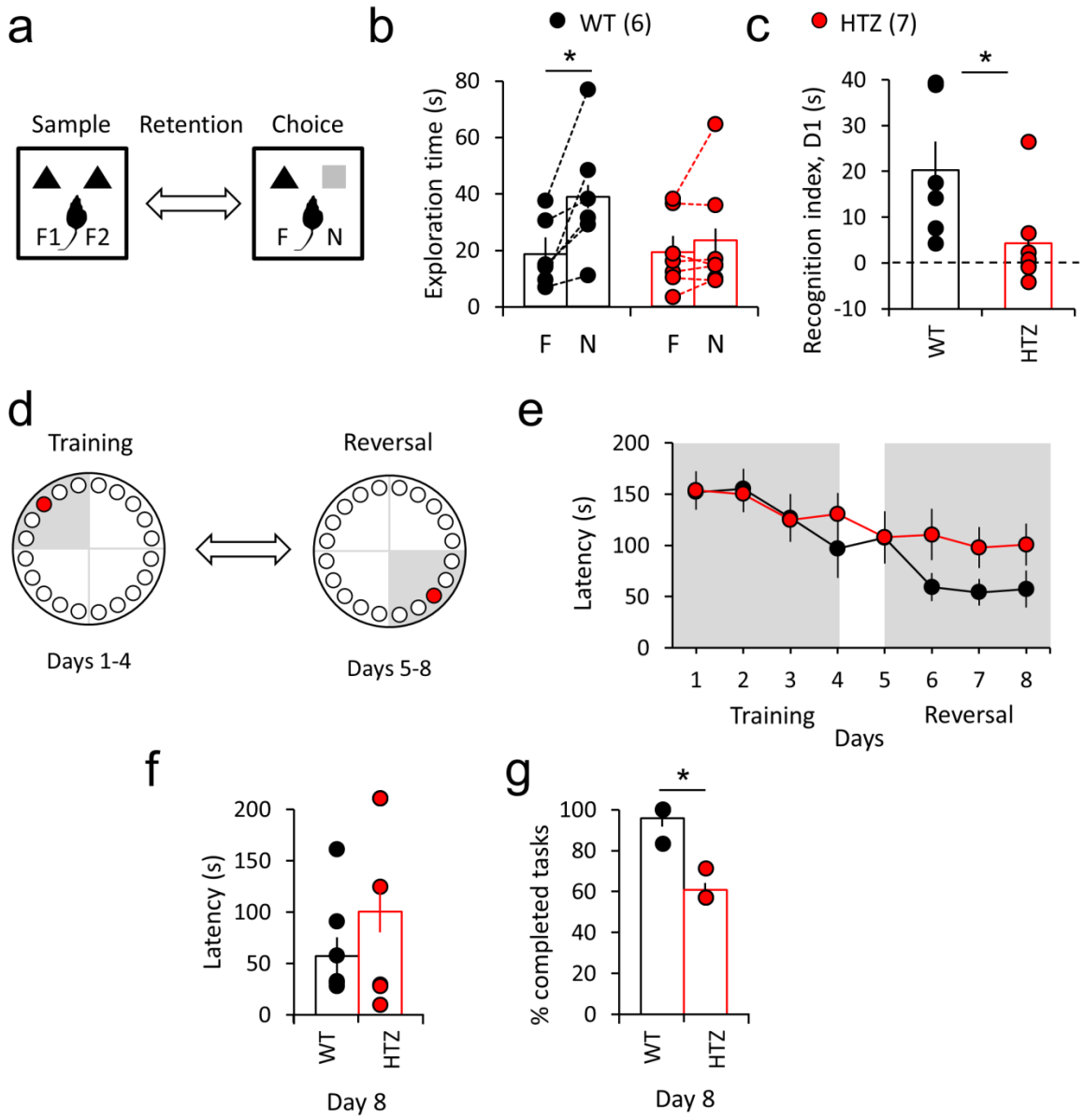

Figure 1: HTZ mice exhibit reduced performance in recognition and spatial memory tasks. WT (black circles) and HTZ (red circles) mice over 6 m.o were evaluated in the novel object recognition (NOR) and the Barnes maze tests to estimate recognition and spatial memory, respectively. **(a)** Representative scheme of the NOR test. Mice are faced with two identical objects (F1 and F2) in the sample phase and then in the choice phase, the objects are replaced by an extra copy of the familiar object (F) and a novel object (N). **(b)** Mean exploration time for familial (F) and novel (N) objects. Note that HTZ mice spend significantly less time exploring new objects compared to WT mice. Wilcoxon test, *p =0.0312 compared to the WT condition. **(c)** Mean recognition index (D1). Positive values indicate recognition of the novel over the familial object. Mann-Whitney test, *p =0.0221 compared to the WT condition **(d)** Schematic representation of the BM test. Mice were trained for 4 days to find and escape to a hidden dark box using visual cues (Training phase). On the fifth day, the escape box is located in the opposing quadrant keeping the visual cues to evaluate spatial memory flexibility (Reversal phase). **(e)** Quantification of the latency to entry into the escape box throughout the training and reversal sessions.

(f) Mean latency to entry into the escape box at day 8 of the test (last day of the reversal phase). **(6)** Quantification of the percentage of animals that completed the task at the end of the reversal phase. Note that the the time to enter into the escape box was not statistically significant, but the percentage of HTZ mice that completed the task on the last day of the reversal phase was significantly lower than WT. Mann-Whitney test, *p =0.0286 compared to the WT condition All data are represented as mean ± SEM. In parentheses is the number of WT and HTZ mice.

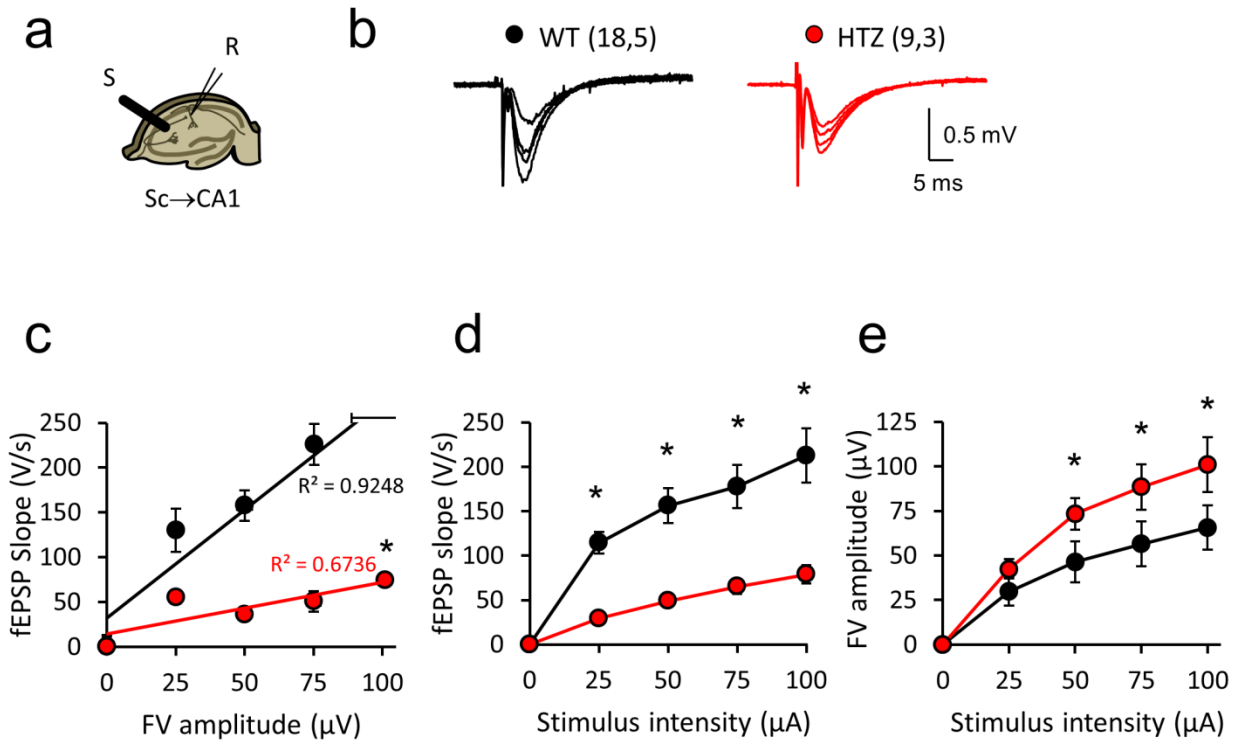

Figure 2: Impaired basal excitatory synaptic transmission in HTZ hippocampal slices **(a)** Scheme of the experimental configuration for field recordings in Schaffer Collaterals (Sc) to CA1 hippocampal synapses. The stimulation electrode and the recording electrode (R) were positioned in *stratum radiatum* of CA1. **(b)** Representative fEPSP traces of both experimental groups HTZ (red) and WT (black**).** The numbers in parentheses are slices, animals recorded. **c)** Relationship between the slope values of fEPSPs and the amplitude of FVs obtained between each experimental groups. The R^2 values for the respective linear regressions are shown. **(d)** Mean fEPSP slopes at different intensity values are plotted per each experimental group. Note the significant difference in fEPSPs as the intensity of stimulation increased between WT and HTZ slices. **(e)** Mean FV amplitudes for WT and HTZ slices. Note the significant difference in FV amplitudes between WT and HTZ slices as the stimulus intensity increased. (WT: n = 18 slices, 5 mice; HTZ: n = 9 slices, 3 mice). All data are represented as mean ± SEM. Statistical differences were calculated using a t-test, * $p < 0.0001$ compared to the WT condition.

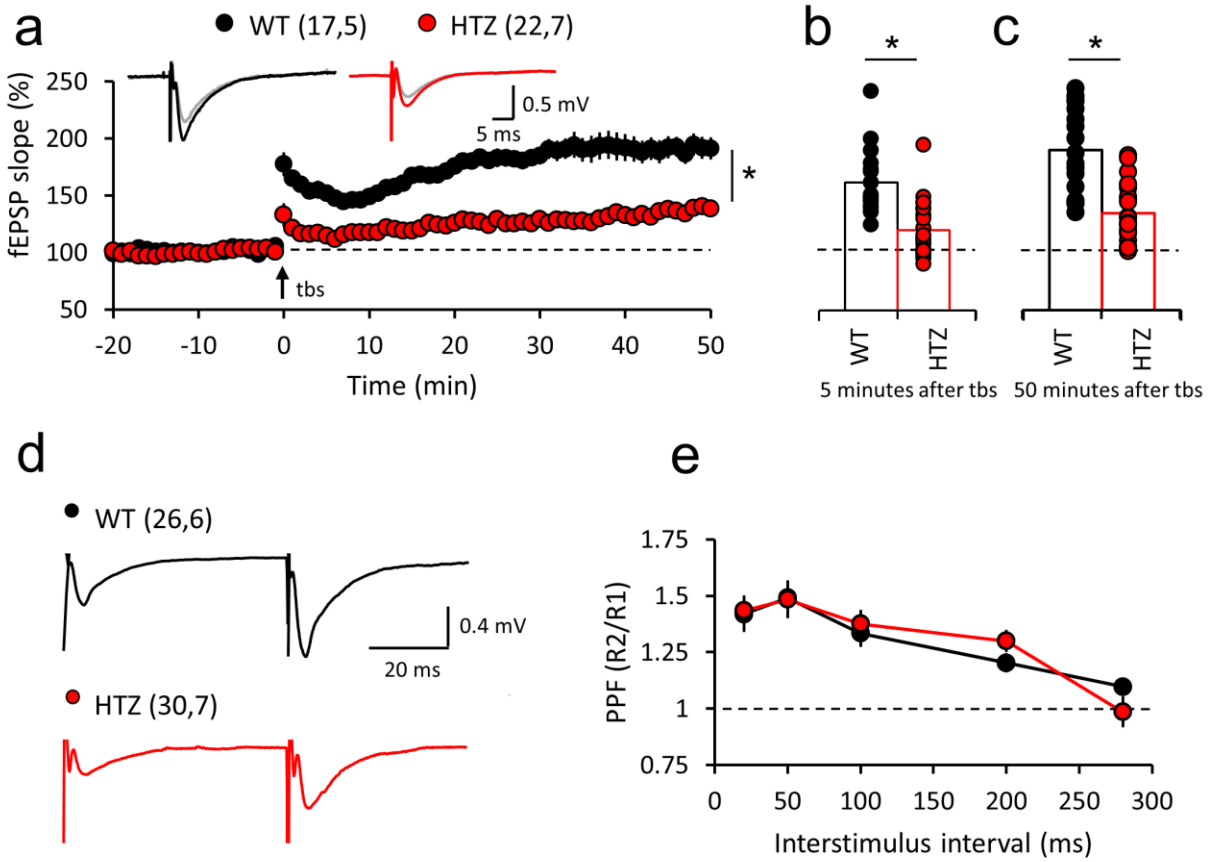

Figure 3: TBS-induced LTP impairment in excitatory synapses of HTZ hippocampal slices. **(a-c)** Hippocampal slices of 6 m.o of WT (black circles) and HTZ (red circles) mice were stimulated with a standard TBS protocol to induce LTP and excitatory postsynaptic field potentials (fEPSP) were recorded during 50 min after the application of the TBS protocol. 2-Way ANOVA, $F_{(1,2257)} = 1414$, *p <0.0001 followed by Bonferroni post hoc test ($p < 0.05$) compared to the WT condition. Representative traces before (gray) and after (black and red) the application of TBS are shown as inserts. Note that at the end of the recording (c), as well as after 5 min of LTP-induction (b) HTZ slices exhibited a significantly reduced potentiation of the synaptic strength compared to WT slices (WT: n = 17 slices, 5 mice; HTZ: n = 22 slices, 7 mice). Mann-Whitney test, *p <0.0001 compared to the WT condition in both 5 or 50 min after TBS. The numbers in parentheses are slices, animals recorded **(d)** Representative traces of HTZ (red) and WT (black) slices stimulated with two stimuli of the same intensity separated by a time of 50 ms for PPF index estimation. Note that the amplitude of the second response was greater than the first one in both cases. **(e)** Paired pulse facilitation by different stimulation intervals. Note that no significant differences were observed between the experimental groups (WT: n = 26, slices 6 mice; HTZ: n = 30 slices, 7 mice). All data are represented as mean ± SEM.

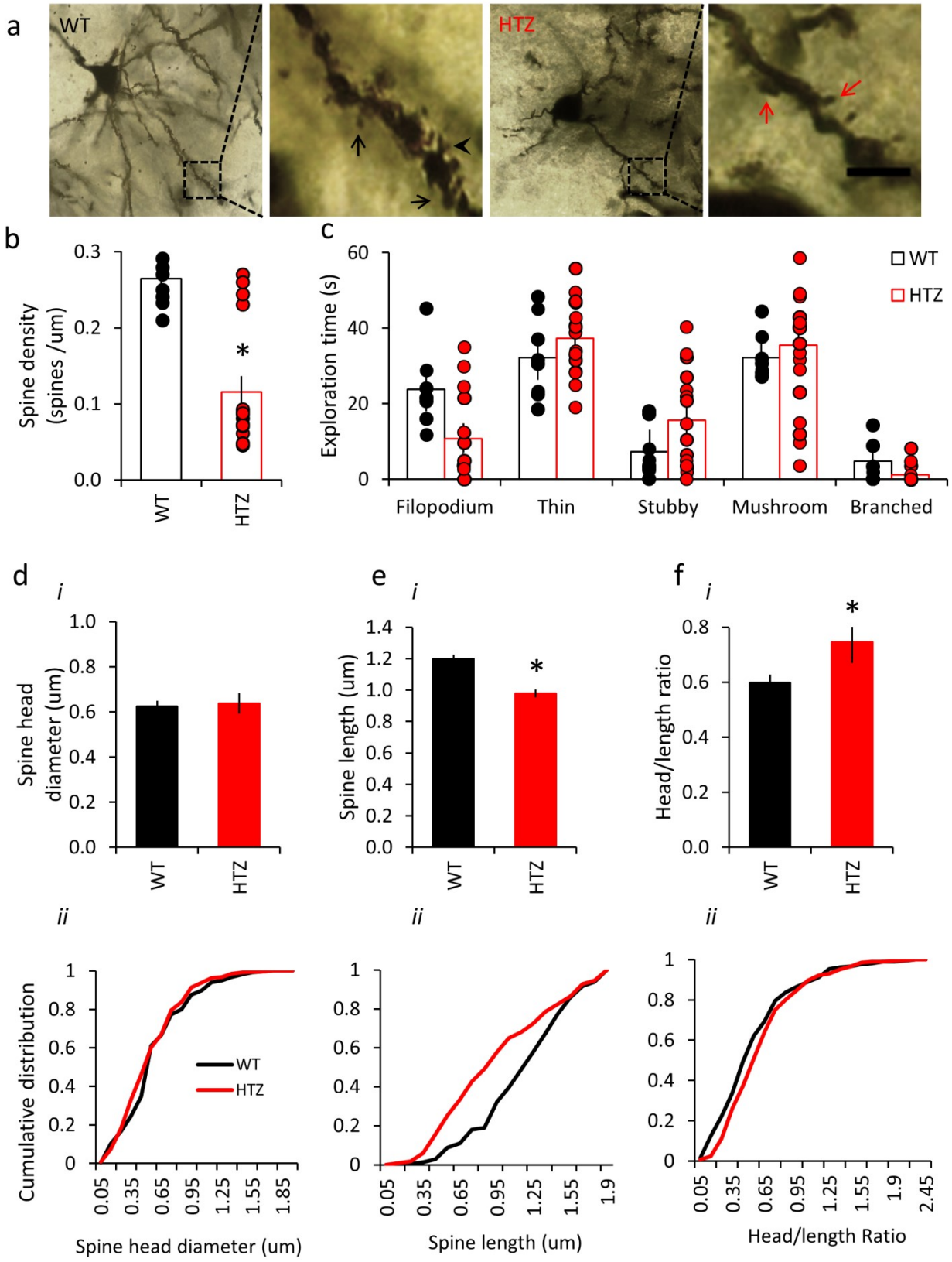
a
WT
HTZ
b
Spine density (spines /um)
0.3
0.2
0.1
0.0
*
WT
HTZ
c
Exploration time (s)
60
40
20
0
WT
HTZ
Filopodium
Thin
Stubby
Mushroom
Branched
d
i
Spine head diameter (um)
1.0
0.8
0.6
0.4
0.2
0.0
WT
HTZ
ii
Cumulative distribution
1
0.8
0.6
0.4
0.2
0
WT
HTZ
0.05
0.35
0.65
0.95
1.25
1.55
1.85
Spine head diameter (um)
e
i
Spine length (um)
1.4
1.2
1.0
0.8
0.6
0.4
0.2
0.0
*
WT
HTZ
ii
1
0.8
0.6
0.4
0.2
0
0.05
0.35
0.65
0.95
1.25
1.55
1.9
Spine length (um)
f
i
Head/length ratio
0.8
0.6
0.4
0.2
0.0
*
WT
HTZ
ii
1
0.8
0.6
0.4
0.2
0
0.05
0.35
0.65
0.95
1.25
1.55
1.9
2.45
Head/length Ratio

618

619 **Figure 4**: Reduced spine density and spine length in hippocampal neurons from adult HTZ brains. Brains
620 from WT (black bars) and HTZ (red bars) mice over 6 m.o were isolated and Golgi-stained for
621 visualization of pyramidal hippocampal neurons **(a)** Representative neurons and dendritic shafts per
622 genotype. Black and red arrows point spines in WT and HTZ dendrites respectively. Black arrowhead
623 highlights a branched spine. Scale bar= 2.5 µm **(b)** Mean spine density per neuron (number of spines per
624 1 µm of dendritic segment) **(c)** Mean percentage of filopodium, thin, stubby, mushroom and branched
625 spines in WT and HTZ hippocampal neurons. 4 dendritic shafts per neuron were analyzed. N=8 WT
626 neurons and 19 HTZ neurons from at least 2 different animals per genotype. Bars are mean ± SEM **(d-f)**
627 Average (i) and cumulative distribution (ii) of spine head diameters (d), spine lengths (e) and
628 head/length ratios (f) in WT and HTZ Golgi-stained neurons. N=217 WT spines, 332 HTZ spines. *$p<0.005$
629 versus WT condition, Mann-Whitney 2-tail test for non-parametric data.

630

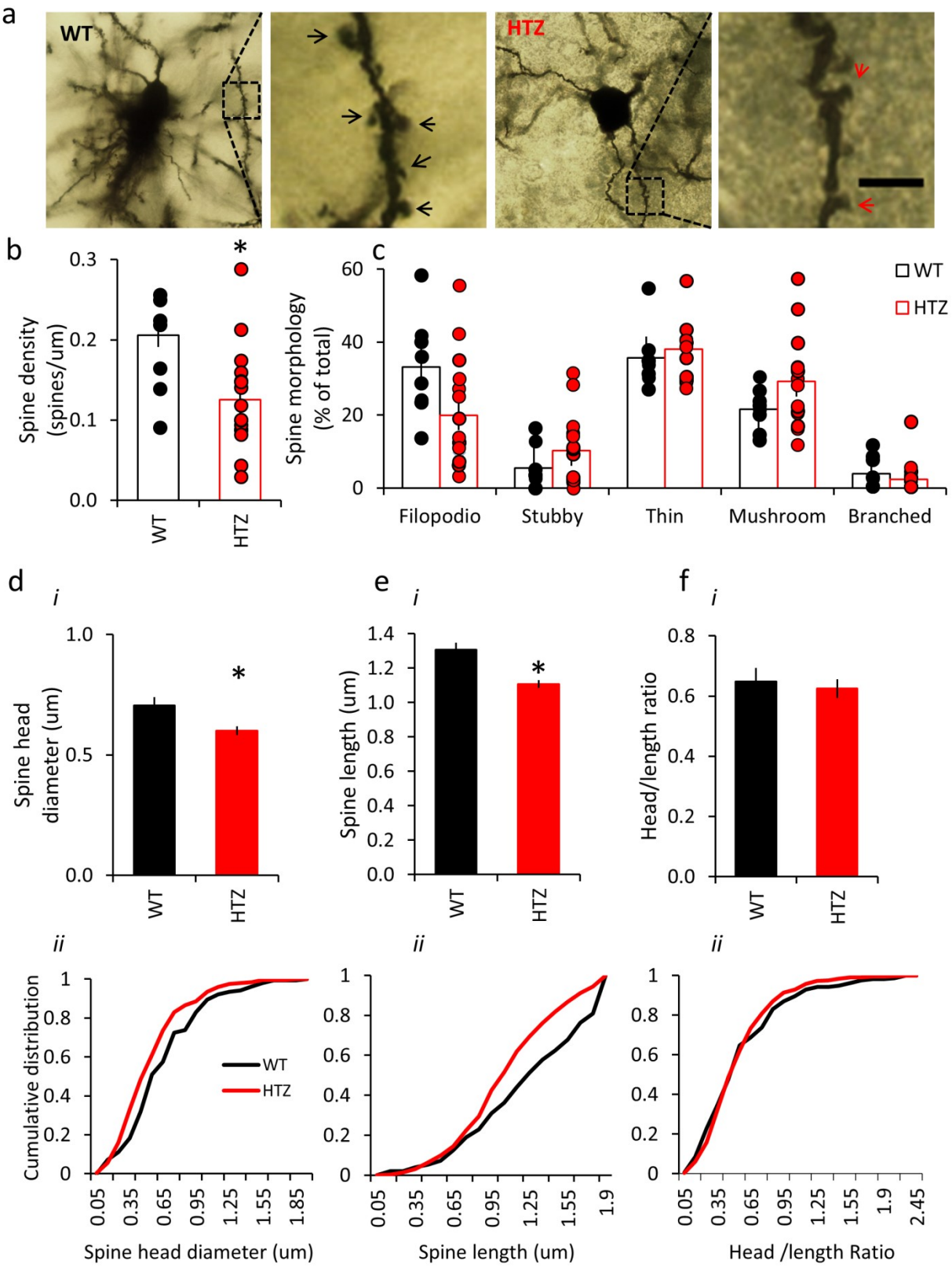
a
WT
HTZ
b
Spine density (spines/um)
0.3
0.2
0.1
0.0
*
WT
HTZ
c
Spine morphology (% of total)
60
40
20
0
WT
HTZ
Filopodio
Stubby
Thin
Mushroom
Branched
d
i
Spine head diameter (um)
1.0
0.5
0.0
*
WT
HTZ
ii
Cumulative distribution
1
0.8
0.6
0.4
0.2
0
WT
HTZ
0.05
0.35
0.65
0.95
1.25
1.55
1.85
Spine head diameter (um)
e
i
Spine length (um)
1.4
1.2
1.0
0.8
0.6
0.4
0.2
0.0
*
WT
HTZ
ii
0.05
0.35
0.65
0.95
1.25
1.55
1.9
Spine length (um)
f
i
Head/length ratio
0.8
0.6
0.4
0.2
0.0
WT
HTZ
ii
0.05
0.35
0.65
0.95
1.25
1.55
1.9
2.45
Head /length Ratio

631
632

Figure 5: Reduced spine density and spine head diameter in cortical neurons from adult HTZ brains. Brains from WT (black bars) and HTZ (red bars) mice over 6 m.o were isolated and Golgi- stained for visualization of pyramidal cortical neurons **(a)** Representative neurons and dendritic shafts per genotype. Black and red arrows point spines in WT and HTZ dendrites respectively. Scale bar= 2.5 µm **(b)** Mean spine density per neuron **(c)** Mean percentage of filopodium, thin, stubby, mushroom or branched spines in WT and HTZ cortical neurons. 4 dendritic shafts per neuron were analyzed N= 8 WT neurons and 19 HTZ neurons from at least two different animals per genotype. Bars are mean ± SEM **(d-f)** Average (i) and cumulative distribution (ii) of spine head diameters (d), spine lengths (e) and head/length ratios (f) in WT and HTZ Golgi-stained neurons. N=155 WT spines, 328 HTZ spines. *$p<0.005$ versus WT condition, Mann-Whitney 2-tail test for non-parametric data.

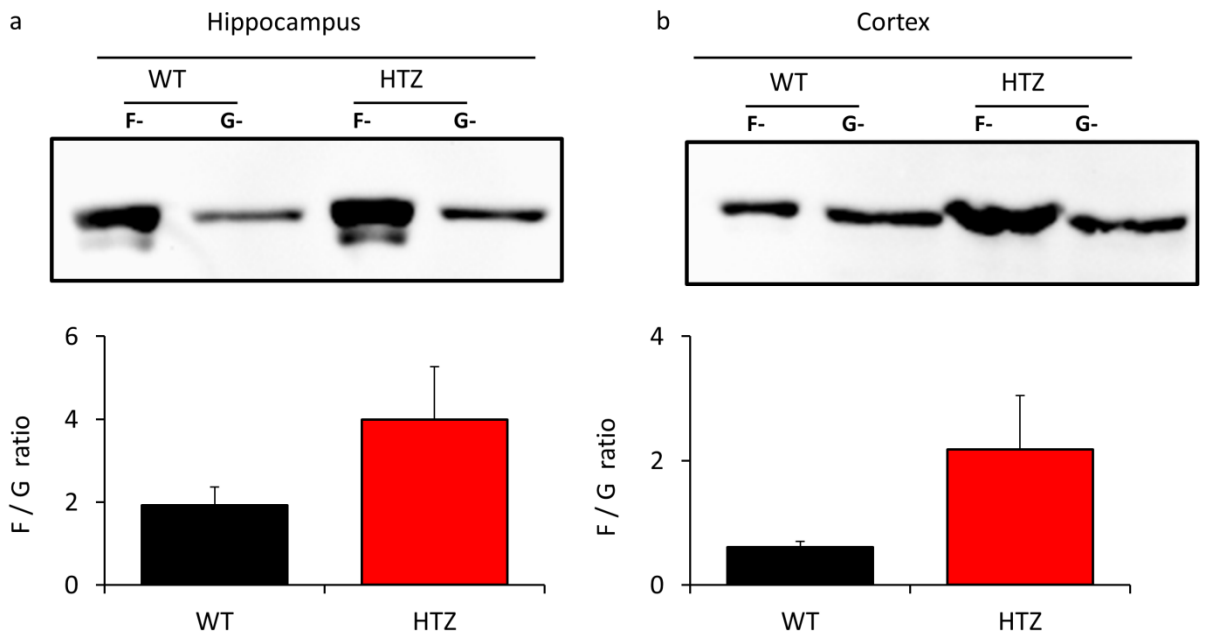

Figure 6: Imbalance in the F/G actin ratio in brains of HTZ mice. Representative blots of the relative amounts of F- and G-actin in the hippocampus (a) and cortex (b) of WT and HTZ mice are shown at the top. Graphs below summarize the quantification of the densitometry analysis of the F/G actin ratio in hippocampus (a) and cortex (b) isolated from WT and HTZ mouse brains. Bars are mean ± SEM of tissues from 3 WT and 3 HTZ mice. Statistical comparison was done using Mann-Whitney test for non-parametric data. p=0.200 and 0.400 for hippocampus and cortex, respectively. Although not significant HTZ brain tissue tended to exhibit an increased F/G ratio compared to the WT condition.

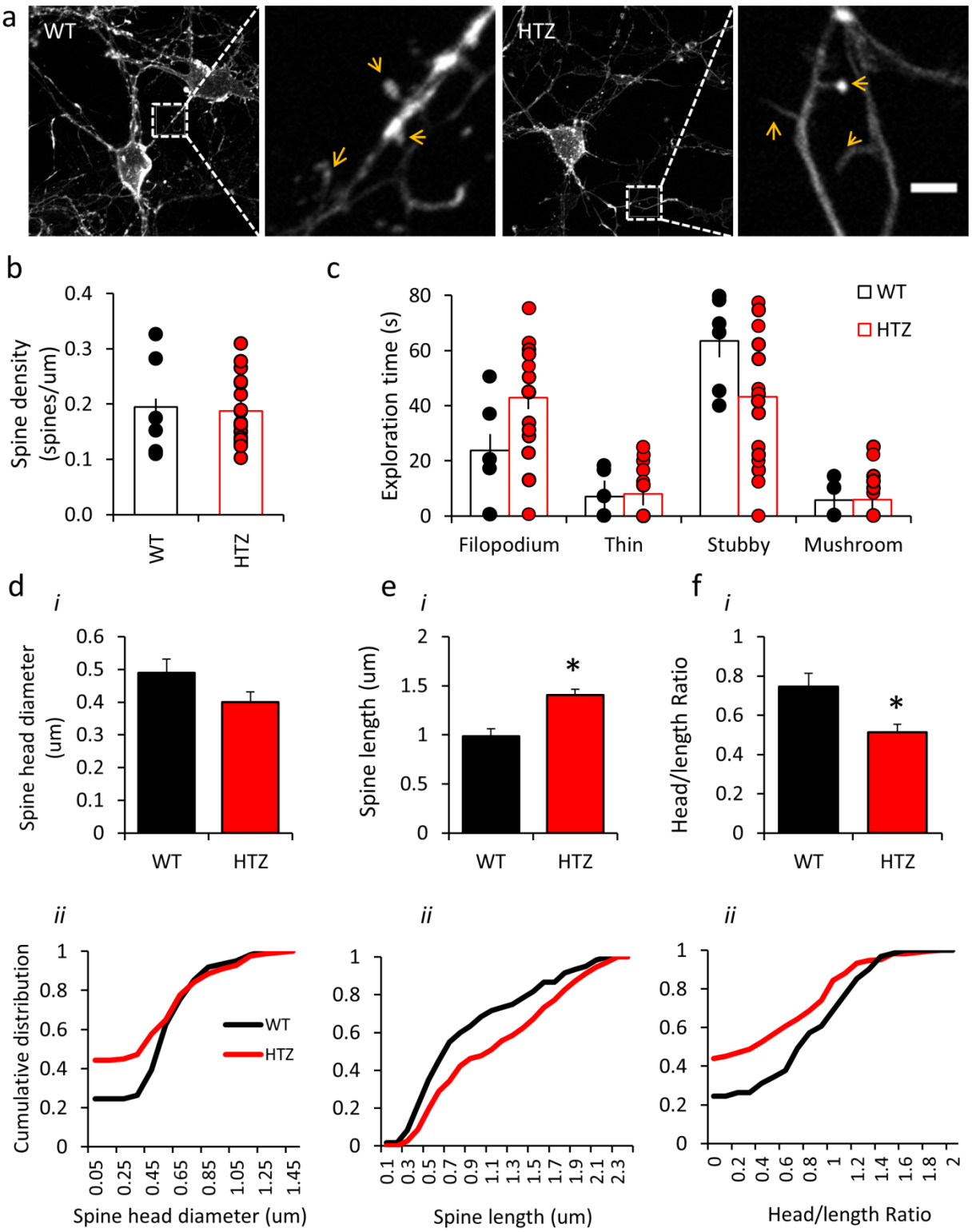
a
WT
HTZ
b
Spine density (spines/um)
0.4
0.3
0.2
0.1
0.0
WT
HTZ
c
Exploration time (s)
80
60
40
20
0
WT
HTZ
Filopodium
Thin
Stubby
Mushroom
d
i
Spine head diameter (um)
0.6
0.5
0.4
0.3
0.2
0.1
0
WT
HTZ
ii
Cumulative distribution
1
0.8
0.6
0.4
0.2
0
WT
HTZ
0.05
0.25
0.45
0.65
0.85
1.05
1.25
1.45
Spine head diameter (um)
e
i
Spine length (um)
2
1.5
1
0.5
0
*
WT
HTZ
ii
0.1
0.3
0.5
0.7
0.9
1.1
1.3
1.5
1.7
1.9
2.1
2.3
Spine length (um)
f
i
Head/length Ratio
1
0.8
0.6
0.4
0.2
0
*
WT
HTZ
ii
0
0.2
0.4
0.6
0.8
1
1.2
1.4
1.6
1.8
2
Head/length Ratio

678 **Figure 7**: Reduced spine head/length ratio in cultured HTZ neurons. 7 *DIV* hippocampal neurons, primary
679 cultured from WT and HTZ pups (P0), were fixed, stained with the F-actin binding toxin phalloidin-
680 rhodamin-B and visualized by confocal microscopy **(a)** Representative phalloidin-stained neurons and
681 dendritic shafts per genotype. Yellow arrows point typical dendritic spines. Scale bar= 1.5 µm **(b)** Mean
682 spine density per neuron **(c)** Mean percentage of filopodium, thin, stubby or mushroom spines in WT
683 and HTZ phalloidin-stained neurons. Branched spines were not observed neither in WT nor in HTZ
684 neurons. 3 dendritic shafts per neuron N= 3 WT neurons and 18 HTZ neurons from 2 different cultures.
685 Bars are mean ± SEM **(d-f)** Average (i) and cumulative distribution (ii) of spine head diameters (d), spine
686 lengths (e) and head/length ratios (f) in WT and HTZ phalloidin-stained neurons. N=61 WT spines, 166
687 HTZ spines. *$p<0.005$ versus WT condition, Mann-Whitney 2-tail test for non-parametric data.
688
689
690
691
692
693
694
695
696
697
698
699
700
701
702
703
704
705
706

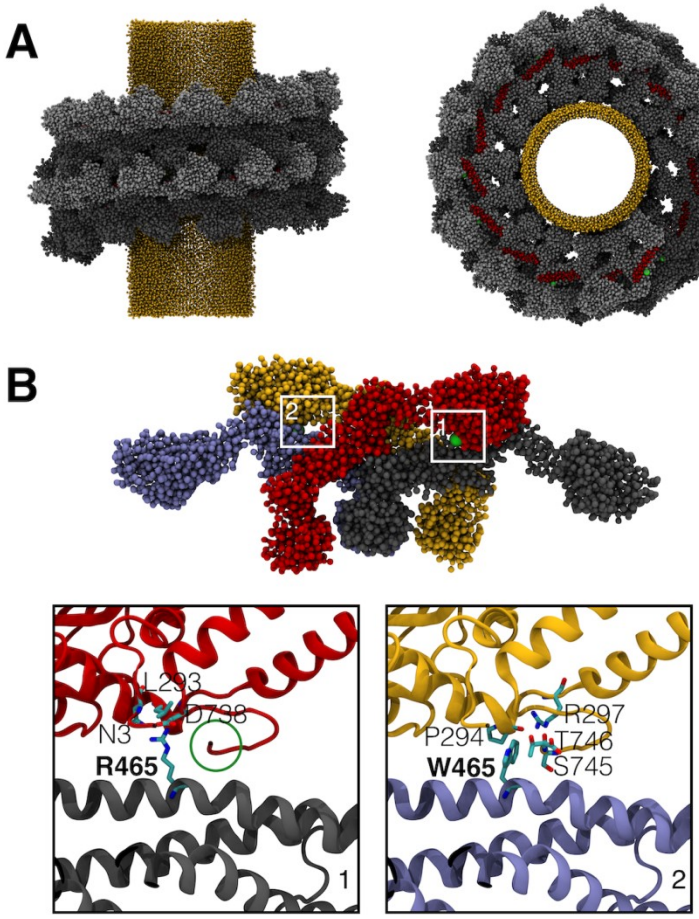

Figure 8: The CNM-causing p.R465W mutation localizes near to a putative direct actin-binding motif in dynamin-2 **(a)** Corse-grained model of a dynamin-2 helix surrounding a lipid nanotube. Dynamin-2 is represented in silver and gray; Putative actin-binding region proposed by Gu et al., (2010) (residues 399 to 444 in the middle domain) are shown in red; the residue R/W465 is represented in green and the lipid nanotube in yellow. **(b)** Tetramer configuration in the dynamin-2 helix. G-domains are colored in blue, BSEs are represented in yellow, stalks are shown in red and PH domains in lime. The position of PRD is represented only in two dynamins-2 as a silver circles. Green dot represent R/W465. **(c)** Amino acids of the BSE that are close to the R/W465. This interaction occurs in a zone close to the PRD. **(d)** G-domains and BSE of WT and mutant dynamin-2. The extension of BSE in the mutant dynamin-2 changes the position of the G-domain.

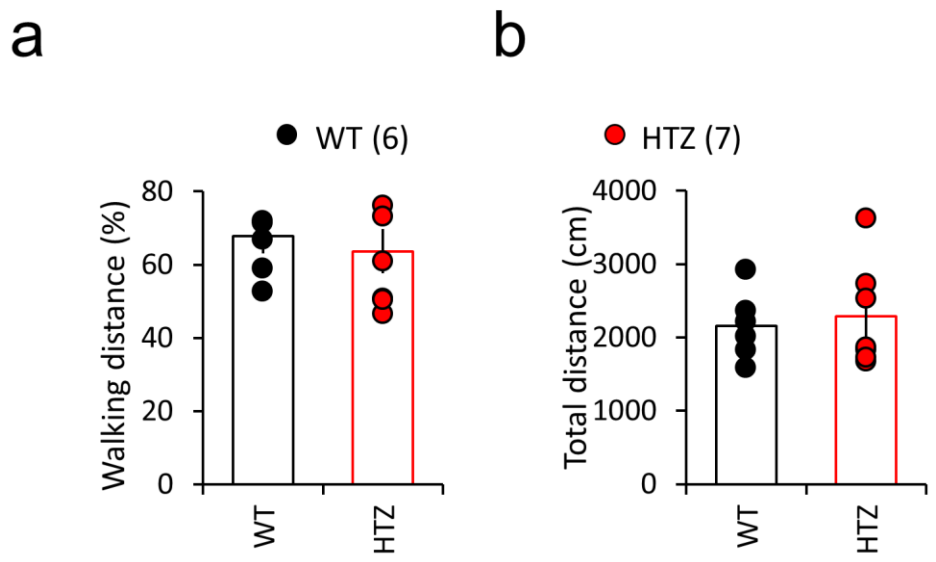

721
722 **Figure S1**: Locomotion activity is not different between WT and HTZ mice. WT (black circles) and HTZ
723 (red circles) mice over 6 m.o were left to explore freely in an open field arena during 5 min. (a) Mean
724 percentage of the walking time and (b) total distance traveled are plotted per each experimental group.
725 All data are represented as mean ± SEM. N= 6 WT and 7 HTZ mice. Statistical differences were
726 calculated using a non-parametric Mann-Whitney test.
727
728
729
730
731
732
733
734
735
736
737
738
739
740
741
742
743
744
745

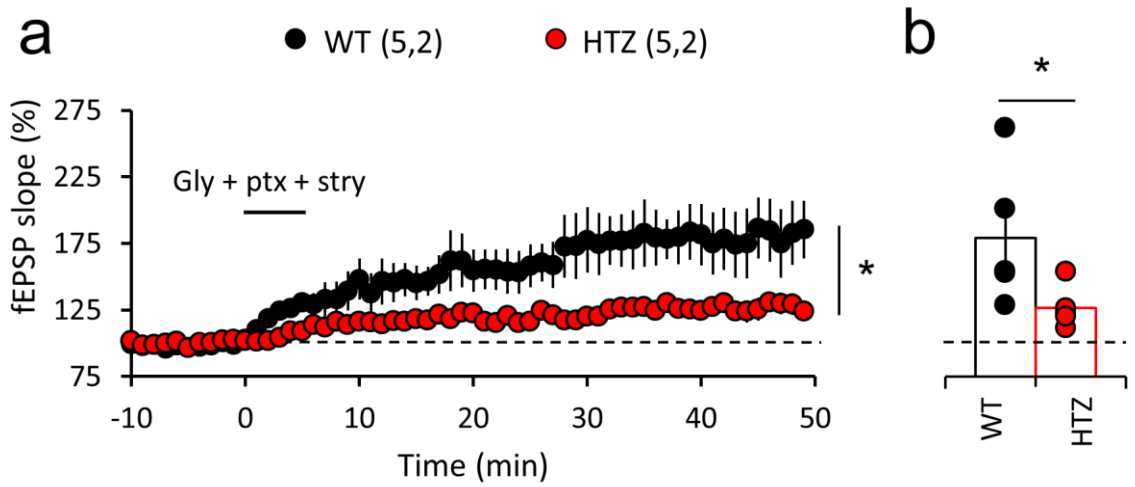

Figure S2: Impaired glycine-induced LTP in HTZ hippocampal slices. **(a-b)** Hippocampal slices from 6 m.o WT (black circles) and HTZ (red circles) mice were stimulated with the application of 600 µM glycine + 50 µM PTX + 3 µM strychnine in order to chemically induce LTP and fEPSPs were recorded during 50 min. 2-Way ANOVA, $F_{(1,480)} = 208.2$, *p <0.0001 followed by Bonferroni post hoc test ($p < 0.05$) compared to the WT condition. Representative traces before (gray) and after (black and red) the application of glycine solution are shown as inserts. Note that HTZ hippocampal slices exhibit a significantly reduced potentiation at the end of the recording (b) compared to the WT slices (N= 5 slices, 2 WT mice; 5 slices, 2 HTZ mice). Mann-Whitney test * p <0.005 compared to the WT condition. All data are represented as mean ± SEM.

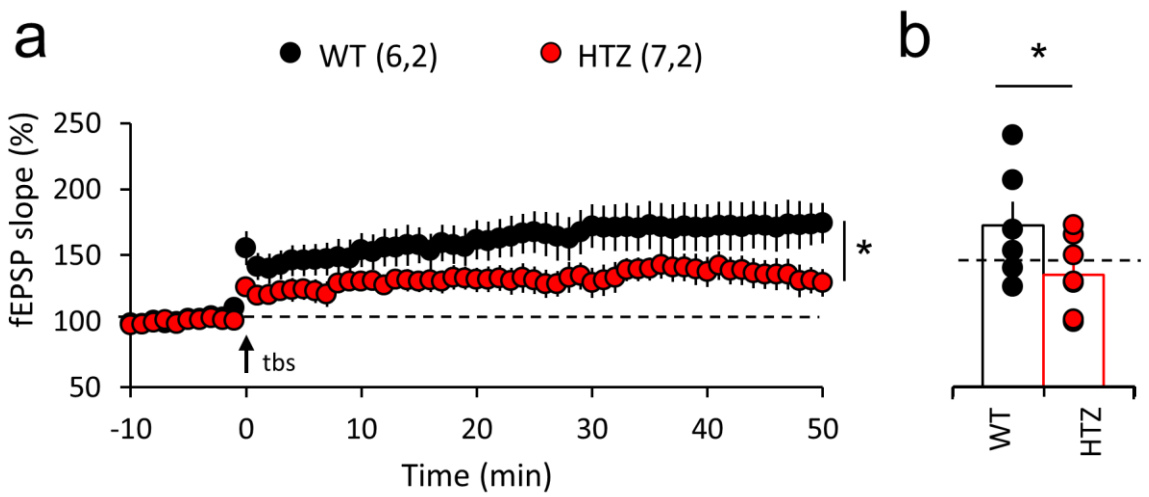

Figure S3. LTP impairment in HTZ hippocampal slices is independent of inhibitory synaptic transmission. **(a-b)** Hippocampal slices from 6 m.o WT (black circles) and HTZ (red circles) mice were stimulated with a standard TBS protocol in the presence of the GABAR-inhibitor Picrotoxin (PTX). fEPSPs were recorded during 50 min after TBS-application. 2-Way ANOVA, $F_{(1,671)} = 245.8$, *p <0.0001 followed by Bonferroni post hoc test ($p < 0.05$) compared to the WT condition. Representative traces before (gray) and after TBS are shown as inserts. Note that even in the presence of PTX, HTZ hippocampal slices exhibit a significantly reduced potentiation compared to WT slices, suggesting that inhibitory transmission is not involved in the synaptic plasticity defects in HTZ slices. N= 6 slices, 2 WT mice/ 7 slices, 2 HTZ mice). Mann-Whitney test * p <0.005 compared to the WT condition. All data are represented as mean ± SEM.

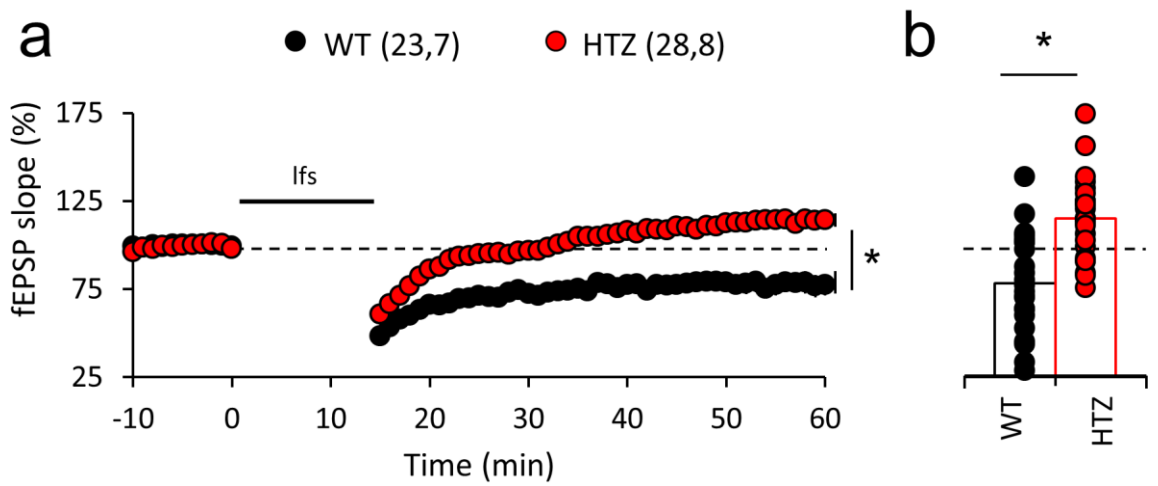

Figure S4. Impaired LFS-induced LTD in HTZ hippocampal slices. **(a-b)** Hippocampal slices from 6 m.o WT (black circles) and HTZ (red circles) mice were stimulated with a standard low-frequency electrical stimulation (LFS) protocol and fEPSPs were recorded during 60 min to estimate depression of the synaptic response (LTD). 2-Way ANOVA, $F_{(1,2793)} = 1039$, *$p < 0.0001$ followed by Bonferroni post hoc test ($p < 0.05$) compared to the WT condition. Representative traces before (gray) and after LFS are shown as inserts. Note that HTZ hippocampal slices exhibit a significantly reduced capability to depress the synaptic response at the end of the recording compared to WT slices (WT: n = 23 slices, 7 mice; HTZ: n = 28 slices, 8 mice). Mann-Whitney test * $p < 0.005$ compared to the WT condition. All data are represented as mean ± SEM.

.

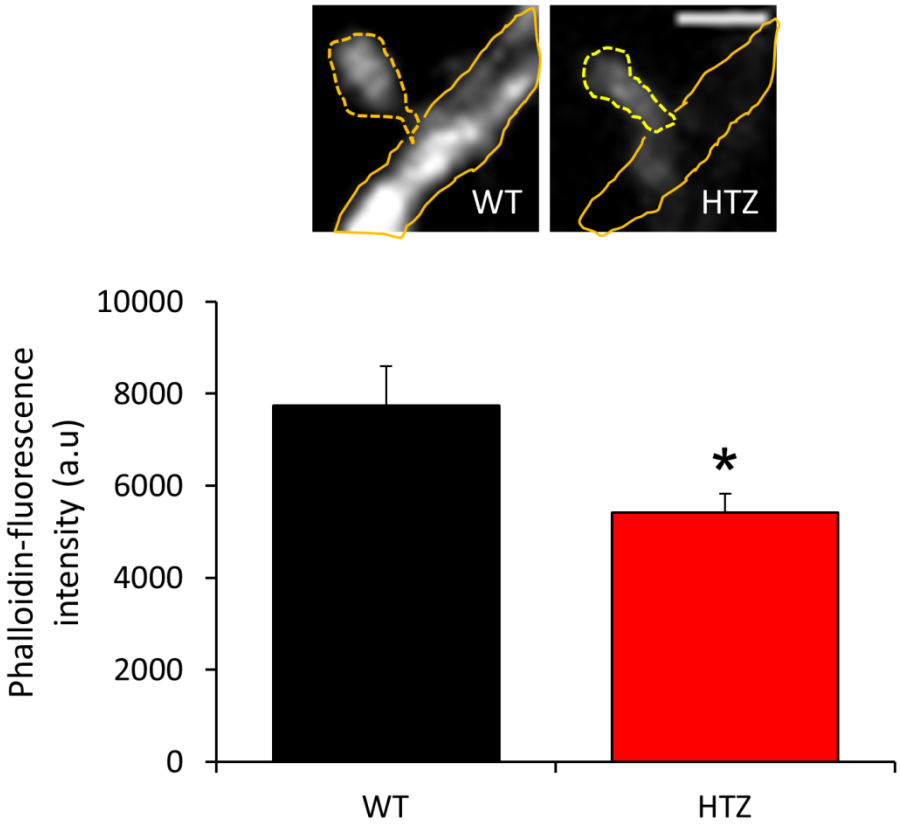

Figure S5. Reduced phalloidin-reactivity in dendritic spines of HTZ neurons. 7 *DIV* hippocampal neurons, cultured from WT and HTZ pups (P0), were fixed, stained with the F-actin binding toxin phalloidin-rhodamin-B and visualized by confocal microscopy using the same acquisition parameters **(a)** Representative phalloidin-stained WT and HTZ dendritic spines are shown above. Dotted yellow lines draw the spine perimeters. Phalloidin fluorescence intensity was measured inside spines. Scale bar= 1.5 µm **(b)** Mean phalloidin-fluorescence intensity in WT (black bar) and HTZ (red bar) dendritic spines. N=61 WT spines and 166 HTZ from 3 WT and 18 HTZ neurons. Bars are mean ± SEM *$p<0.0002$ compared to WT condition, Mann-Whitney 2-tail test for non-parametric data.

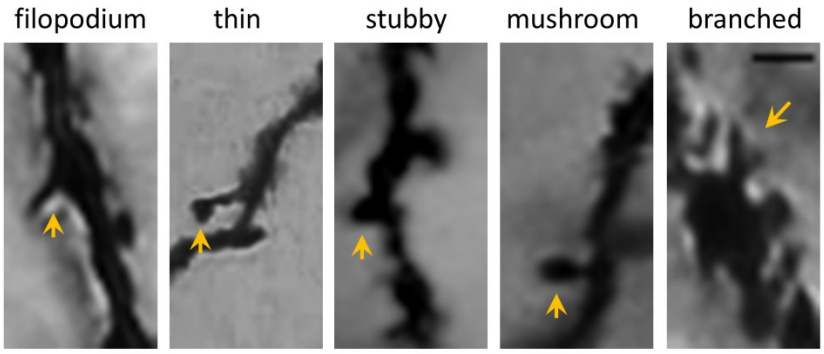

Figure S6. Representative dendritic spine-morphologies. Filopodia are long protrusions (> 2 um) without head. Thin-spines are short (<2 um) protrusions with small heads (<0.5 um). Stubby-spines are wide-head protrusions without neck. Mushroom spines are short protrusions (<1 um) with wide-heads (> 0.6 um width). Branched spines are short cup-shaped protrussions. Yellow arrows point dendritic spines of each morphology. Scale bar=2 um

838 **References**

839 Ali, Tayyibah, Joanna Bednarska, Stéphane Vassilopoulos, Martin Tran, Ivan A. Diakonov, Azza Ziyadeh-
840 Isleem, Pascale Guicheney, et al. 2019. "Correlative SICM-FCM Reveals Changes in Morphology and
841 Kinetics of Endocytic Pits Induced by Disease-Associated Mutations in Dynamin." *FASEB Journal* 33
842 (7): 8504–18. https://doi.org/10.1096/fj.201802635R.

843 Anggono, Victor, and Richard L. Huganir. 2012a. "Regulation of AMPA Receptor Trafficking and Synaptic
844 Plasticity." *Current Opinion in Neurobiology*. Curr Opin Neurobiol.
845 https://doi.org/10.1016/j.conb.2011.12.006.

846 2012b. "Regulation of AMPA Receptor Trafficking and Synaptic Plasticity." *Current Opinion in*
847 *Neurobiology*. Curr Opin Neurobiol. https://doi.org/10.1016/j.conb.2011.12.006.

848 Antonny, Bruno, Christopher Burd, Pietro De Camilli, Elizabeth Chen, Oliver Daumke, Katja Faelber,
849 Marijn Ford, et al. 2016. "Membrane Fission by Dynamin: What We Know and What We Need to
850 Know." *The EMBO Journal*. https://doi.org/10.15252/embj.201694613.

851 Ardiles, Alvaro O., Carolina Flores-Muñoz, Gabriela Toro-Ayala, Ana M. Cárdenas, Adrian G. Palacios,
852 Pablo Muñoz, Marco Fuenzalida, Juan C. Sáez, and Agustín D. Martínez. 2014. "Pannexin 1
853 Regulates Bidirectional Hippocampal Synaptic Plasticity in Adult Mice." *Frontiers in Cellular*
854 *Neuroscience* 8 (OCT). https://doi.org/10.3389/fncel.2014.00326.

855 Arriagada-Diaz, Jorge, Lorena Prado-Vega, Ana M. Cárdenas Díaz, Alvaro O. Ardiles, and Arlek M.
856 Gonzalez-Jamett. 2020. "Dynamin Superfamily at Pre- and Postsynapses: Master Regulators of
857 Synaptic Transmission and Plasticity in Health and Disease." *Neuroscientist*. SAGE Publications Inc.
858 https://doi.org/10.1177/1073858420974313.

859 Barnes, C. A. 1979. "Memory Deficits Associated with Senescence: A Neurophysiological and Behavioral
860 Study in the Rat." *Journal of Comparative and Physiological Psychology*.
861 https://doi.org/10.1037/h0077579.

862 Bayazitov, Ildar T., Robert J. Richardson, Robert G. Fricke, and Stanislav S. Zakharenko. 2007. "Slow
863 Presynaptic and Fast Postsynaptic Components of Compound Long-Term Potentiation." *Journal of*
864 *Neuroscience* 27 (43): 11510–21. https://doi.org/10.1523/JNEUROSCI.3077-07.2007.

865 Bhatnagar, Anushree, David L. Willins, John A. Gray, Jason Woods, Jeffrey L. Benovic, and Bryan L. Roth.
866 2001. "The Dynamin-Dependent, Arrestin-Independent Internalization of 5-Hydroxytryptamine 2A
867 (5-HT2A) Serotonin Receptors Reveals Differential Sorting of Arrestins and 5-HT2A Receptors
868 during Endocytosis." *Journal of Biological Chemistry*. https://doi.org/10.1074/jbc.M006968200.

869 Bhatnagar, Anushree, David L Willins, John A Gray, Jason Woods, Jeffrey L Benovic, and Bryan L Roth.
870 2000. "The Dynamin-Dependent, Arrestin-Independent Internalization of 5-Hydroxytryptamine 2A
871 (5-HT 2A) Serotonin Receptors Reveals Differential Sorting of Arrestins and 5-HT 2A Receptors
872 during Endocytosis* □ S." *THE JOURNAL OF BIOLOGICAL CHEMISTRY* 276 (11): 8269–77.
873 https://doi.org/10.1074/jbc.M006968200.

874 Bitoun, Marc, Svetlana Maugenre, Pierre Yves Jeannet, Emmanuelle Lacène, Xavier Ferrer, Pascal
875 Laforêt, Jean Jacques Martin, et al. 2005. "Mutations in Dynamin 2 Cause Dominant Centronuclear
876 Myopathy." *Nature Genetics*. https://doi.org/10.1038/ng1657.

877 Bliek, A. M. Van der, T. E. Redelmeier, H. Damke, E. J. Tisdale, E. M. Meyerowitz, and S. L. Schmid. 1993.
878 "Mutations in Human Dynamin Block an Intermediate Stage in Coated Vesicle Formation." *Journal*
879 *of Cell Biology*. https://doi.org/10.1083/jcb.122.3.553.

880 Böhm, Johann, Valerie Biancalana, Elizabeth T. DeChene, Marc Bitoun, Christopher R. Pierson, Elise
881 Schaefer, Hatice Karasoy, et al. 2012. "Mutation Spectrum in the Large Gtpase Dynamin 2, and
882 Genotype-Phenotype Correlation in Autosomal Dominant Centronuclear Myopathy." *Human*
883 *Mutation*. https://doi.org/10.1002/humu.22067.

884 Bosch, Miquel, Jorge Castro, Takeo Saneyoshi, Hitomi Matsuno, Mriganka Sur, and Yasunori Hayashi.
885 2014. "Structural and Molecular Remodeling of Dendritic Spine Substructures during Long-Term
886 Potentiation." *Neuron* 82 (2): 444–59. https://doi.org/10.1016/j.neuron.2014.03.021.

887 Bosch, Miquel, and Yasunori Hayashi. 2012. "Structural Plasticity of Dendritic Spines." *Current Opinion in*
888 *Neurobiology*. Elsevier Current Trends. https://doi.org/10.1016/j.conb.2011.09.002.

889 Carroll, Reed C., Eric C. Beattie, Houhui Xia, Christian Lüscher, Yoram Altschuler, Roger A. Nicoll, Robert
890 C. Malenka, and Mark Von Zastrow. 1999. "Dynamin-Dependent Endocytosis of Ionotropic
891 Glutamate Receptors." *Proceedings of the National Academy of Sciences of the United States of*
892 *America*. https://doi.org/10.1073/pnas.96.24.14112.

893 Chappie, Joshua S., Sharmistha Acharya, Ya Wen Liu, Marilyn Leonard, Thomas J. Pucadyil, and Sandra L.
894 Schmid. 2009. "An Intramolecular Signaling Element That Modulates Dynamin Function in Vitro
895 and in Vivo." *Molecular Biology of the Cell*. https://doi.org/10.1091/mbc.E09-04-0318.

896 Cheung, Giselle, and Michael A. Cousin. 2019. "Synaptic Vesicle Generation from Activity-Dependent
897 Bulk Endosomes Requires a Dephosphorylation-Dependent Dynamin–Syndapin Interaction."
898 *Journal of Neurochemistry* 151 (5): 570–83. https://doi.org/10.1111/jnc.14862.

899 Chowdhury, Shoaib, Jason D. Shepherd, Hiroyuki Okuno, Gregory Lyford, Ronald S. Petralia, Niels Plath,
900 Dietmar Kuhl, Richard L. Huganir, and Paul F. Worley. 2006. "Arc/Arg3.1 Interacts with the
901 Endocytic Machinery to Regulate AMPA Receptor Trafficking." *Neuron* 52 (3): 445–59.
902 https://doi.org/10.1016/j.neuron.2006.08.033.

903 Cingolani, Lorenzo A., Agnes Thalhammer, Lily M.Y. Yu, Myriam Catalano, Timothy Ramos, Michael A.
904 Colicos, and Yukiko Goda. 2008. "Activity-Dependent Regulation of Synaptic AMPA Receptor
905 Composition and Abundance by B3 Integrins." *Neuron* 58 (5): 749–62.
906 https://doi.org/10.1016/j.neuron.2008.04.011.

907 Citri, Ami, and Robert C. Malenka. 2008. "Synaptic Plasticity: Multiple Forms, Functions, and
908 Mechanisms." *Neuropsychopharmacology*. Neuropsychopharmacology.
909 https://doi.org/10.1038/sj.npp.1301559.

910 Damke, Hanna, Takeshi Baba, Dale E. Warnock, and Sandra L. Schmid. 1994. "Induction of Mutant
911 Dynamin Specifically Blocks Endocytic Coated Vesicle Formation." *Journal of Cell Biology*.
912 https://doi.org/10.1083/jcb.127.4.915.

913 Durieux, Anne Cécile, Bernard Prudhon, Pascale Guicheney, and Marc Bitoun. 2010. "Dynamin 2 and
914 Human Diseases." *Journal of Molecular Medicine*. https://doi.org/10.1007/s00109-009-0587-4.

915 Durieux, Anne Cécile, Stéphane Vassilopoulos, Jeanne Lainé, Bodvaël Fraysse, Laura Briñas, Bernard

Prudhon, Josiane Castells, et al. 2012. “A Centronuclear Myopathy - Dynamin 2 Mutation Impairs Autophagy in Mice.” *Traffic* 13 (6): 869–79. https://doi.org/10.1111/j.1600-0854.2012.01348.x.

Durieux, Anne Cécile, Alban Vignaud, Bernard Prudhon, Mai Thao Viou, Maud Beuvin, Stéphane Vassilopoulos, Bodvaël Fraysse, et al. 2010. “A Centronuclear Myopathy-Dynamin 2 Mutation Impairs Skeletal Muscle Structure and Function in Mice.” *Human Molecular Genetics*. https://doi.org/10.1093/hmg/ddq413.

Echaniz-Laguna, Andoni, Anne Sophie Nicot, Sophie Carré, Jérôme Franques, Christine Tranchant, Nicolas Dondaine, Valérie Biancalana, Jean Louis Mandel, and Jocelyn Laporte. 2007. “Subtle Central and Peripheral Nervous System Abnormalities in a Family with Centronuclear Myopathy and a Novel Dynamin 2 Gene Mutation.” *Neuromuscular Disorders*. https://doi.org/10.1016/j.nmd.2007.06.467.

Ennaceur, A., and J. Delacour. 1988. “A New One-Trial Test for Neurobiological Studies of Memory in Rats. 1: Behavioral Data.” *Behavioural Brain Research* 31 (1): 47–59. https://doi.org/10.1016/0166-4328(88)90157-X.

Fa, Mauro, Agnieszka Staniszewski, Faisal Saeed, Yitshak I. Francis, and Ottavio Arancio. 2014. “Dynamin 1 Is Required for Memory Formation.” *PLoS ONE* 9 (3). https://doi.org/10.1371/journal.pone.0091954.

Faelber, Katja, York Posor, Song Gao, Martin Held, Yvette Roske, Dennis Schulze, Volker Haucke, Frank Noé, and Oliver Daumke. 2011. “Crystal Structure of Nucleotide-Free Dynamin.” *Nature*. https://doi.org/10.1038/nature10369.

Ferguson, Shawn M., Gabor Brasnjo, Mitsuko Hayashi, Markus Wölfel, Chiara Collesi, Silvia Giovedi, Andrea Raimondi, et al. 2007. “A Selective Activity-Dependent Requirement for Dynamin 1 in Synaptic Vesicle Endocytosis.” *Science*. https://doi.org/10.1126/science.1140621.

Ferguson, Shawn M., and Pietro De Camilli. 2012. “Dynamin, a Membrane-Remodelling GTPase.” *Nature Reviews Molecular Cell Biology*. https://doi.org/10.1038/nrm3266.

Ferguson, Shawn, Andrea Raimondi, Summer Paradise, Hongying Shen, Kumi Mesaki, Agnes Ferguson, Olivier Destaing, et al. 2009. “Coordinated Actions of Actin and BAR Proteins Upstream of Dynamin at Endocytic Clathrin-Coated Pits.” *Developmental Cell*. https://doi.org/10.1016/j.devcel.2009.11.005.

Fischer, Dirk, Muriel Herasse, Marc Bitoun, Héctor M. Barragán-Campos, Jacques Chiras, Pascal Laforêt, Michel Fardeau, Bruno Eymard, Pascale Guicheney, and Norma B. Romero. 2006. “Characterization of the Muscle Involvement in Dynamin 2-Related Centronuclear Myopathy.” *Brain*. https://doi.org/10.1093/brain/awl071.

Flores-Muñoz, Carolina, Bárbara Gómez, Elena Mery, Paula Mujica, Ivana Gajardo, Claudio Córdova, Daniela Lopez-Espíndola, et al. 2020. “Acute Pannexin 1 Blockade Mitigates Early Synaptic Plasticity Defects in a Mouse Model of Alzheimer’s Disease.” *Frontiers in Cellular Neuroscience* 14 (March). https://doi.org/10.3389/fncel.2020.00046.

Ford, Marijn G.J., Simon Jenni, and Jodi Nunnari. 2011. “The Crystal Structure of Dynamin.” *Nature*. https://doi.org/10.1038/nature10441.

955 Gajardo, Ivana, Claudia S. Salazar, Daniela Lopez-Espíndola, Carolina Estay, Carolina Flores-Muñoz,
956 Claudio Elgueta, Arlek M. Gonzalez-Jamett, Agustín D. Martínez, Pablo Muñoz, and Álvaro O.
957 Ardiles. 2018. "Lack of Pannexin 1 Alters Synaptic GluN2 Subunit Composition and Spatial Reversal
958 Learning in Mice." *Frontiers in Molecular Neuroscience* 11 (April).
959 https://doi.org/10.3389/fnmol.2018.00114.

960 Gipson, C. D., and M. F. Olive. 2017. "Structural and Functional Plasticity of Dendritic Spines – Root or
961 Result of Behavior?" *Genes, Brain and Behavior*. Blackwell Publishing Ltd.
962 https://doi.org/10.1111/gbb.12324.

963 González-Jamett, Arlek M., Ximena Baez-Matus, María José Olivares, Fernando Hinostroza, Maria José
964 Guerra-Fernández, Jacqueline Vasquez-Navarrete, Mai Thao Bui, et al. 2017. "Dynamin-2
965 Mutations Linked to Centronuclear Myopathy Impair Actin-Dependent Trafficking in Muscle Cells."
966 *Scientific Reports*. https://doi.org/10.1038/s41598-017-04418-w.

967 González-Jamett, Arlek M., Fanny Momboisse, María José Guerra, Stéphane Ory, Ximena Báez-Matus,
968 Natalia Barraza, Valerie Calco, et al. 2013. "Dynamin-2 Regulates Fusion Pore Expansion and
969 Quantal Release through a Mechanism That Involves Actin Dynamics in Neuroendocrine
970 Chromaffin Cells." *PLoS ONE*. https://doi.org/10.1371/journal.pone.0070638.

971 González-Jamett, Arlek M., Fanny Momboisse, Valentina Haro-Acuña, Jorge A. Bevilacqua, Pablo
972 Caviedes, and Ana María Cárdenas. 2013. "Dynamin-2 Function and Dysfunction along the
973 Secretory Pathway." *Frontiers in Endocrinology*. https://doi.org/10.3389/fendo.2013.00126.

974 Gu, Changkyu, Suma Yaddanapudi, Astrid Weins, Teresia Osborn, Jochen Reiser, Martin Pollak, John
975 Hartwig, and Sanja Sever. 2010. "Direct Dynaming-Actin Interactions Regulate the Actin
976 Cytoskeleton." *EMBO Journal*. https://doi.org/10.1038/emboj.2010.249.

977 Harris, Kristen M., and S. B. Kater. 1994. "Dendritic Spines: Cellular Specializations Imparting Both
978 Stability and Flexibility to Synaptic Function." *Annual Review of Neuroscience*. Annual Reviews Inc.
979 https://doi.org/10.1146/annurev.ne.17.030194.002013.

980 Hinshaw, Jenny E., and Sandra L. Schmid. 1995. "Dynamin Self-Assembles into Rings Suggesting a
981 Mechanism for Coated Vesicle Budding." *Nature* 374 (6518): 190–92.
982 https://doi.org/10.1038/374190a0.

983 Holtmaat, Anthony, and Karel Svoboda. 2009. "Experience-Dependent Structural Synaptic Plasticity in
984 the Mammalian Brain." *Nature Reviews Neuroscience*. Nat Rev Neurosci.
985 https://doi.org/10.1038/nrn2699.

986 Hotulainen, Pirta, and Casper C. Hoogenraad. 2010. "Actin in Dendritic Spines: Connecting Dynamics to
987 Function." *Journal of Cell Biology* 189 (4): 619–29. https://doi.org/10.1083/jcb.201003008.

988 Jaskolski, Frédéric, Belen Mayo-Martin, David Jane, and Jeremy M. Henley. 2009. "Dynamin-Dependent
989 Membrane Drift Recruits AMPA Receptors to Dendritic Spines." *Journal of Biological Chemistry*.
990 https://doi.org/10.1074/jbc.M808401200.

991 Jeannet, P. Y., G. Bassez, B. Eymard, P. Laforêt, J. A. Urtizberea, A. Rouche, P. Guicheney, M. Fardeau,
992 and Norma Beatriz Romero. 2004. "Clinical and Histologic Findings in Autosomal Centronuclear
993 Myopathy." *Neurology*. https://doi.org/10.1212/01.WNL.0000124388.67003.56.

994 Kabbani, Nadine, Andreas Jeromin, and Robert Levenson. 2004. "Dynamin-2 Associates with the
995 Dopamine Receptor Signalplex and Regulates Internalization of Activated D2 Receptors." *Cellular*
996 *Signalling*. https://doi.org/10.1016/j.cellsig.2003.09.011.

997 Kim, Chong Hyun, and John E. Lisman. 1999. "A Role of Actin Filament in Synaptic Transmission and
998 Long-Term Potentiation." *Journal of Neuroscience* 19 (11): 4314–24.
999 https://doi.org/10.1523/jneurosci.19-11-04314.1999.

1000 Kong, Leopold, Kem A. Sochacki, Huaibin Wang, Shunming Fang, Bertram Canagarajah, Andrew D. Kehr,
1001 William J. Rice, Marie Paule Strub, Justin W. Taraska, and Jenny E. Hinshaw. 2018. "Cryo-EM of the
1002 Dynamin Polymer Assembled on Lipid Membrane." *Nature* 560 (7717): 258–62.
1003 https://doi.org/10.1038/s41586-018-0378-6.

1004 Koutsopoulos, Olga S., Catherine Koch, Valerie Tosch, Johann Böhm, Kathryn N. North, and Jocelyn
1005 Laporte. 2011. "Mild Functional Differences of Dynamin 2 Mutations Associated to Centronuclear
1006 Myopathy and Charcot-Marie-Tooth Peripheral Neuropathy." Edited by Gisela Nogales-Gadea.
1007 *PLoS ONE* 6 (11): e27498. https://doi.org/10.1371/journal.pone.0027498.

1008 Lee, Hey Kyoung, and Alfredo Kirkwood. 2011. "AMPA Receptor Regulation during Synaptic Plasticity in
1009 Hippocampus and Neocortex." *Seminars in Cell and Developmental Biology*. Elsevier Ltd.
1010 https://doi.org/10.1016/j.semcdb.2011.06.007.

1011 Lin, Shan Shan, Tsung Lin Hsieh, Gunn Guang Liou, Tsai Ning Li, Hsin Chieh Lin, Chiung Wen Chang,
1012 Hsiang Yi Wu, Chi Kuang Yao, and Ya Wen Liu. 2020. "Dynamin-2 Regulates Postsynaptic
1013 Cytoskeleton Organization and Neuromuscular Junction Development." *Cell Reports* 33 (4).
1014 https://doi.org/10.1016/j.celrep.2020.108310.

1015 Liu, Ya Wen, Vasyl Lukiyanchuk, and Sandra L. Schmid. 2011. "Common Membrane Trafficking Defects of
1016 Disease-Associated Dynamin 2 Mutations." *Traffic*. https://doi.org/10.1111/j.1600-
1017 0854.2011.01250.x.

1018 Loerke, Dinah, Marcel Mettlen, Defne Yarar, Khuloud Jaqaman, Henry Jaqaman, Gaudenz Danuser, and
1019 Sandra L. Schmid. 2009. "Cargo and Dynamin Regulate Clathrin-Coated Pit Maturation." *PLoS*
1020 *Biology*. https://doi.org/10. 1371/journal.pbio.1000057.

1021 Lomash, Richa Madan, Xinglong Gu, Richard J. Youle, Wei Lu, and Katherine W. Roche. 2015.
1022 "Neurolastin, a Dynamin Family GTPase, Regulates Excitatory Synapses and Spine Density." *Cell*
1023 *Reports* 12 (5): 743–51. https://doi.org/10.1016/j.celrep.2015.06.064.

1024 Lu, Jiuyi, Thomas D. Helton, Thomas A. Blanpied, Bence Rácz, Thomas M. Newpher, Richard J. Weinberg,
1025 and Michael D. Ehlers. 2007. "Postsynaptic Positioning of Endocytic Zones and AMPA Receptor
1026 Cycling by Physical Coupling of Dynamin-3 to Homer." *Neuron* 55 (6): 874–89.
1027 https://doi.org/10.1016/j.neuron.2007.06.041.

1028 Lu, Wei Yang, Heng Ye Man, William Ju, William S. Trimble, John F. MacDonald, and Yu Tian Wang. 2001.
1029 "Activation of Synaptic NMDA Receptors Induces Membrane Insertion of New AMPA Receptors
1030 and LTP in Cultured Hippocampal Neurons." *Neuron* 29 (1): 243–54.
1031 https://doi.org/10.1016/S0896-6273(01)00194-5.

1032 Malenka, Robert C., and Mark F. Bear. 2004. "LTP and LTD: An Embarrassment of Riches." *Neuron*.
1033 Neuron. https://doi.org/10.1016/j.neuron.2004.09.012.

1034 Matsuzaki, Masanori, Graham C.R. Ellis-Davies, Tomomi Nemoto, Yasushi Miyashita, Masamitsu Iino,
1035 and Haruo Kasai. 2001. “Dendritic Spine Geometry Is Critical for AMPA Receptor Expression in
1036 Hippocampal CA1 Pyramidal Neurons.” *Nature Neuroscience* 4 (11): 1086–92.
1037 https://doi.org/10.1038/nn736.

1038 Matus, A. 2000. “Actin-Based Plasticity in Dendritic Spines.” *Science*. Science.
1039 https://doi.org/10.1126/science.290.5492.754.

1040 Mooren, Olivia L., Tatyana I. Kotova, Andrew J. Moore, and Dorothy A. Schafer. 2009. “Dynamin2 GTPase
1041 and Cortactin Remodel Actin Filaments.” *Journal of Biological Chemistry*.
1042 https://doi.org/10.1074/jbc.M109.024398.

1043 Moro, Alessandro., van Nifterick Ann., Toonen Ruud., Verhage Matthijs. 2021. "Dynamin controls
1044 neuropeptides secretion by organizing dense-core vesicle fusion sites"Science Advances. https://DOI:
1045 10.1126/sciadv.abf0659

1046 Negrón-Oyarzo, Ignacio, David Neira, Nelson Espinosa, Pablo Fuentealba, and Francisco Aboitiz. 2015.
1047 “Prenatal Stress Produces Persistence of Remote Memory and Disrupts Functional Connectivity in
1048 the Hippocampal-Prefrontal Cortex Axis.” *Cerebral Cortex*. https://doi.org/10.1093/cercor/bhu108.

1049 Newman-Smith, Erin D., Dixie Lee Shurland, and Alexander M. Van Der Bliek. 1997. “Assignment of the
1050 Dynamin-1 Gene (DNM1) to Human Chromosome 9q34 by Fluorescence in Situ Hybridization and
1051 Somatic Cell Hybrid Analysis.” *Genomics*. https://doi.org/10.1006/geno.1996.4596.

1052 Nicoziani, Paolo, Frederik Vilhardt, Alicia Llorente, Leila Hilout, Pierre J. Courtoy, Kirsten Sandvig, and Bo
1053 Van Deurs. 2000. “Role for Dynamin in Late Endosome Dynamics and Trafficking of the Cation-
1054 Independent Mannose 6-Phosphate Receptor.” *Molecular Biology of the Cell*.
1055 https://doi.org/10.1091/mbc.11.2.481.

1056 Noakes, P. G., D. Chin, S. S. Kim, S. Liang, and W. D. Phillips. 1999. “Expression and Localisation of
1057 Dynamin and Syntaxin during Neural Development and Neuromuscular Synapse Formation.”
1058 *Journal of Comparative Neurology*. https://doi.org/10.1002/(SICI)1096-
1059 9861(19990809)410:4<531::AID-CNE2>3.0.CO;2-C.

1060 Okamoto, Ken Ichi, Takeharu Nagai, Atsushi Miyawaki, and Yasunori Hayashi. 2004. “Rapid and
1061 Persistent Modulation of Actin Dynamics Regulates Postsynaptic Reorganization Underlying
1062 Bidirectional Plasticity.” *Nature Neuroscience* 7 (10): 1104–12. https://doi.org/10.1038/nn1311.

1063 Okamoto, Kenichi, Miquel Bosch, and Yasunori Hayashi. 2009. “The Roles of CaMKII and F-Actin in the
1064 Structural Plasticity of Dendritic Spines: A Potential Molecular Identity of a Synaptic Tag?”
1065 *Physiology* 24 (6): 357–66. https://doi.org/10.1152/physiol.00029.2009.

1066 Okamoto, Patricia M., Chantal Gamby, David Wells, Justin Fallon, and Richard B. Vallee. 2001. “Dynamin
1067 Isoform-Specific Interaction with the Shank/ProSAP Scaffolding Proteins of the Postsynaptic
1068 Density and Actin Cytoskeleton.” *Journal of Biological Chemistry*.
1069 https://doi.org/10.1074/jbc.M104927200.

1070 Pelucchi, Silvia, Ramona Stringhi, and Elena Marcello. 2020. “Dendritic Spines in Alzheimer’s Disease:
1071 How the Actin Cytoskeleton Contributes to Synaptic Failure.” *International Journal of Molecular*
1072 *Sciences*. MDPI AG. https://doi.org/10.3390/ijms21030908.

1073 Penzes, Peter, and Igor Rafalovich. 2012. “Regulation of the Actin Cytoskeleton in Dendritic Spines.”
1074 *Advances in Experimental Medicine and Biology* 970: 81–95. https://doi.org/10.1007/978-3-7091-
1075 0932-8_4.

1076 Pitts, Matthew. 2018. “Barnes Maze Procedure for Spatial Learning and Memory in Mice.” *BIO-*
1077 *PROTOCOL*. https://doi.org/10.21769/bioprotoc.2744.

1078 Praefcke, Gerrit J.K., and Harvey T. McMahon. 2004. “The Dynamin Superfamily: Universal Membrane
1079 Tubulation and Fission Molecules?” *Nature Reviews Molecular Cell Biology*.
1080 https://doi.org/10.1038/nrm1313.

1081 Raimondi, Andrea, Shawn M. Ferguson, Xuelin Lou, Moritz Armbruster, Summer Paradise, Silvia Giovedi,
1082 Mirko Messa, et al. 2011. “Overlapping Role of Dynamin Isoforms in Synaptic Vesicle Endocytosis.”
1083 *Neuron*. https://doi.org/10.1016/j.neuron.2011.04.031.

1084 Romero, Norma B., and Marc Bitoun. 2011. “Centronuclear Myopathies.” *Seminars in Pediatric*
1085 *Neurology* 18 (4): 250–56. https://doi.org/10.1016/j.spen.2011.10.006.

1086 Schiffer, Mario, Beina Teng, Changkyu Gu, Valentina A. Shchedrina, Marina Kasaikina, Vincent A. Pham,
1087 Nils Hanke, et al. 2015. “Pharmacological Targeting of Actin-Dependent Dynamin Oligomerization
1088 Ameliorates Chronic Kidney Disease in Diverse Animal Models.” *Nature Medicine* 21 (6): 601–9.
1089 https://doi.org/10.1038/nm.3843.

1090 Shin, Wonchul, Lihao Ge, Gianvito Arpino, Seth A. Villarreal, Edaeni Hamid, Huisheng Liu, Wei Dong
1091 Zhao, Peter J. Wen, Hsueh Cheng Chiang, and Ling Gang Wu. 2018. “Visualization of Membrane
1092 Pore in Live Cells Reveals a Dynamic-Pore Theory Governing Fusion and Endocytosis.” *Cell* 173 (4):
1093 934-945.e12. https://doi.org/10.1016/j.cell.2018.02.062.

1094 Shors, Tracey J., and Louis D. Matzel. 1997. “Long-Term Potentiation: What’s Learning Got to Do with
1095 It?” *Behavioral and Brain Sciences*. Behav Brain Sci. https://doi.org/10.1017/S0140525X97001593.

1096 Singh, Mahaveer, Hemant R. Jadhav, and Tanya Bhatt. 2017. “Dynamin Functions and Ligands: Classical
1097 Mechanisms Behind.” *Molecular Pharmacology*. https://doi.org/10.1124/mol.116.105064.

1098 Stefen, Holly, Chanchanok Chaichim, John Power, and Thomas Fath. 2016. “Regulation of the
1099 Postsynaptic Compartment of Excitatory Synapses by the Actin Cytoskeleton in Health and Its
1100 Disruption in Disease.” *Neural Plasticity* 2016. https://doi.org/10.1155/2016/2371970.

1101 Sukoff Rizzo, Stacey J., and Jacqueline N. Crawley. 2017. “Behavioral Phenotyping Assays for Genetic
1102 Mouse Models of Neurodevelopmental, Neurodegenerative, and Psychiatric Disorders.” *Annual*
1103 *Review of Animal Biosciences*. https://doi.org/10.1146/annurev-animal-022516-022754.

1104 Tanabe, Kenji, and Kohji Takei. 2009. “Dynamic Instability of Microtubules Requires Dynamin 2 and Is
1105 Impaired in a Charcot-Marie-Tooth Mutant.” *Journal of Cell Biology*.
1106 https://doi.org/10.1083/jcb.200803153.

1107 Tanifuji, Shota, Megumi Funakoshi-Tago, Fumihito Uedas, Tadashi Kasaharas, and Sumiko Mochida.
1108 2013. “Dynamin Isoforms Decode Action Potential Firing for Synaptic Vesicle Recycling.” *Journal of*
1109 *Biological Chemistry*. https://doi.org/10.1074/jbc.M112.445874.

1110 Wang, Weisheng, Yun Yue Ju, Qi Xin Zhou, Jian Xin Tang, Meng Li, Lei Zhang, Shuo Kang, et al. 2017. “The

1111 Small GTPase Rac1 Contributes to Extinction of Aversive Memories of Drug Withdrawal by
1112 Facilitating GABAa Receptor Endocytosis in the VmPFC." *Journal of Neuroscience*.
1113 https://doi.org/10.1523/JNEUROSCI.3859-16.2017.

1114 Warnock, Dale E., Takeshi Baba, and Sandra L. Schmid. 1997. "Ubiquitously Expressed Dynamin-II Has a
1115 Higher Intrinsic GTPase Activity and a Greater Propensity for Self-Assembly than Neuronal
1116 Dynamin-I." *Molecular Biology of the Cell*. https://doi.org/10.1091/mbc.8.12.2553.

1117 Watanabe, Shigeki, Benjamin R. Rost, Marcial Camacho-Pérez, M. Wayne Davis, Berit Söhl-Kielczynski,
1118 Christian Rosenmund, and Erik M. Jorgensen. 2013. "Ultrafast Endocytosis at Mouse Hippocampal
1119 Synapses." *Nature* 504 (7479): 242–47. https://doi.org/10.1038/nature12809.

1120 Yamada, Hiroshi, Tadashi Abe, Ayano Satoh, Nana Okazaki, Shota Tago, Kinue Kobayashi, Yumi Yoshida,
1121 et al. 2013. "Stabilization of Actin Bundles by a Dynamin 1/Cortactin Ring Complex Is Necessary for
1122 Growth Cone Filopodia." *Journal of Neuroscience* 33 (10): 4514–26.
1123 https://doi.org/10.1523/JNEUROSCI.2762-12.2013.

1124 Zhang, Ruihui, Donghoon M. Lee, John R. Jimah, Nathalie Gerassimov, Changsong Yang, Sangjoon Kim,
1125 Delgermaa Luvsanjav, et al. 2020. "Dynamin Regulates the Dynamics and Mechanical Strength of
1126 the Actin Cytoskeleton as a Multifilament Actin-Bundling Protein." *Nature Cell Biology* 22 (6): 674–
1127 88. https://doi.org/10.1038/s41556-020-0519-7.

1128 Zhang, Xiao Yan, Fang Ji, Ning Wang, Lin Lin Chen, Tian Tian, and Wei Lu. 2014. "Glycine Induces
1129 Bidirectional Modifications in N-Methyl-D-Aspartate Receptor-Mediated Synaptic Responses in
1130 Hippocampal CA1 Neurons." *Journal of Biological Chemistry* 289 (45): 31200–211.
1131 https://doi.org/10.1074/jbc.M114.570630.

1132 Zheng, Ning, Okunola Jeyifous, Charlotte Munro, Johanna M. Montgomery, and William N. Green. 2015.
1133 "Synaptic Activity Regulates AMPA Receptor Trafficking through Different Recycling Pathways."
1134 *ELife* 4 (MAY). https://doi.org/10.7554/eLife.06878.

1135 Züchner, Stephan, Maher Noureddine, Marina Kennerson, Kristien Verhoeven, Kristl Claeys, Peter De
1136 Jonghe, John Merory, et al. 2005. "Mutations in the Pleckstrin Homology Domain of Dynamin 2
1137 Cause Dominant Intermediate Charcot-Marie-Tooth Disease." *Nature Genetics*.
1138 https://doi.org/10.1038/ng1514.

1139 Zucker, Robert S., and Wade G. Regehr. 2002. "Short-Term Synaptic Plasticity." *Annual Review of*
1140 *Physiology*. Annu Rev Physiol. https://doi.org/10.1146/annurev.physiol.64.092501.114547.

1141

1142

1143

1144

1145

1146

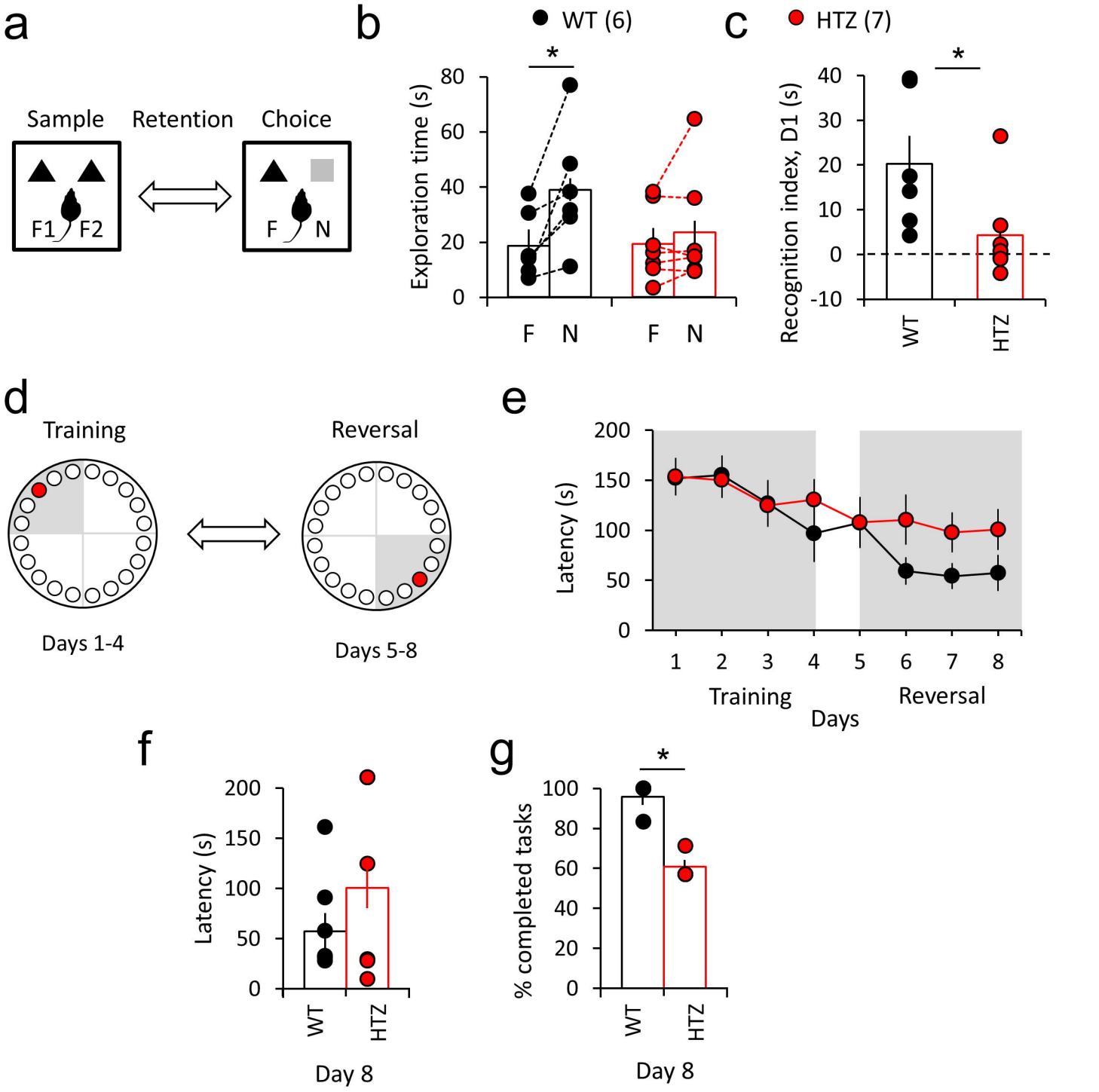
a
Sample
Retention
Choice
F1
F2
F
N
b
WT (6)
*
Exploration time (s)
80
60
40
20
0
F
N
F
N
c
HTZ (7)
*
Recognition index, D1 (s)
40
30
20
10
0
-10
WT
HTZ
d
Training
Reversal
Days 1-4
Days 5-8
e
Latency (s)
200
150
100
50
0
1
2
3
4
5
6
7
8
Training
Reversal
Days
f
Latency (s)
200
150
100
50
0
WT
HTZ
Day 8
g
*
% completed tasks
100
80
60
40
20
0
WT
HTZ
Day 8

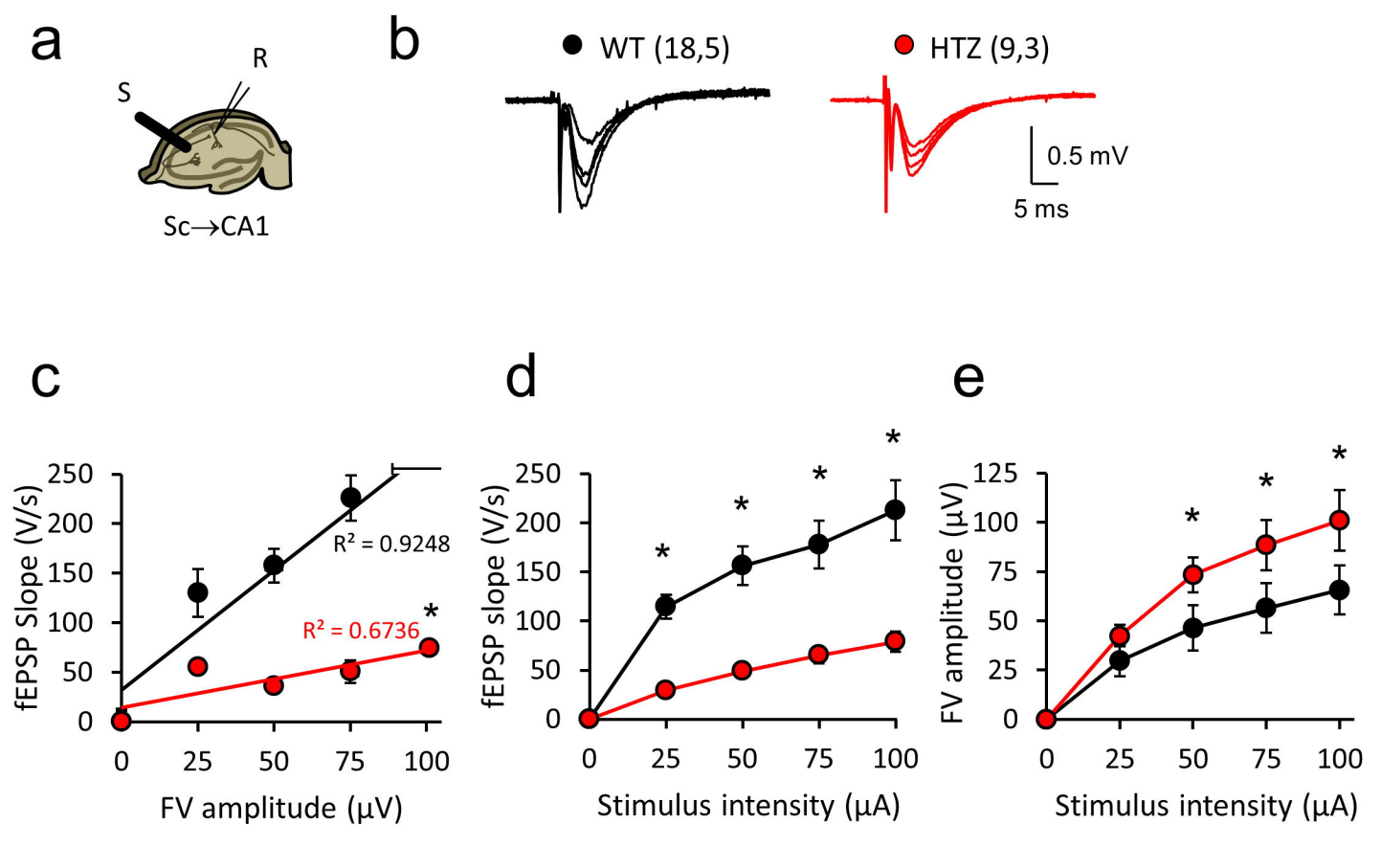
a
S
R
Sc→CA1
b
WT (18,5)
HTZ (9,3)
0.5 mV
5 ms
c
fEPSP Slope (V/s)
250
200
150
100
50
0
R² = 0.9248
R² = 0.6736
*
0
25
50
75
100
FV amplitude (µV)
d
fEPSP slope (V/s)
250
200
150
100
50
0
*
*
*
*
0
25
50
75
100
Stimulus intensity (µA)
e
FV amplitude (µV)
125
100
75
50
25
0
*
*
*
0
25
50
75
100
Stimulus intensity (µA)

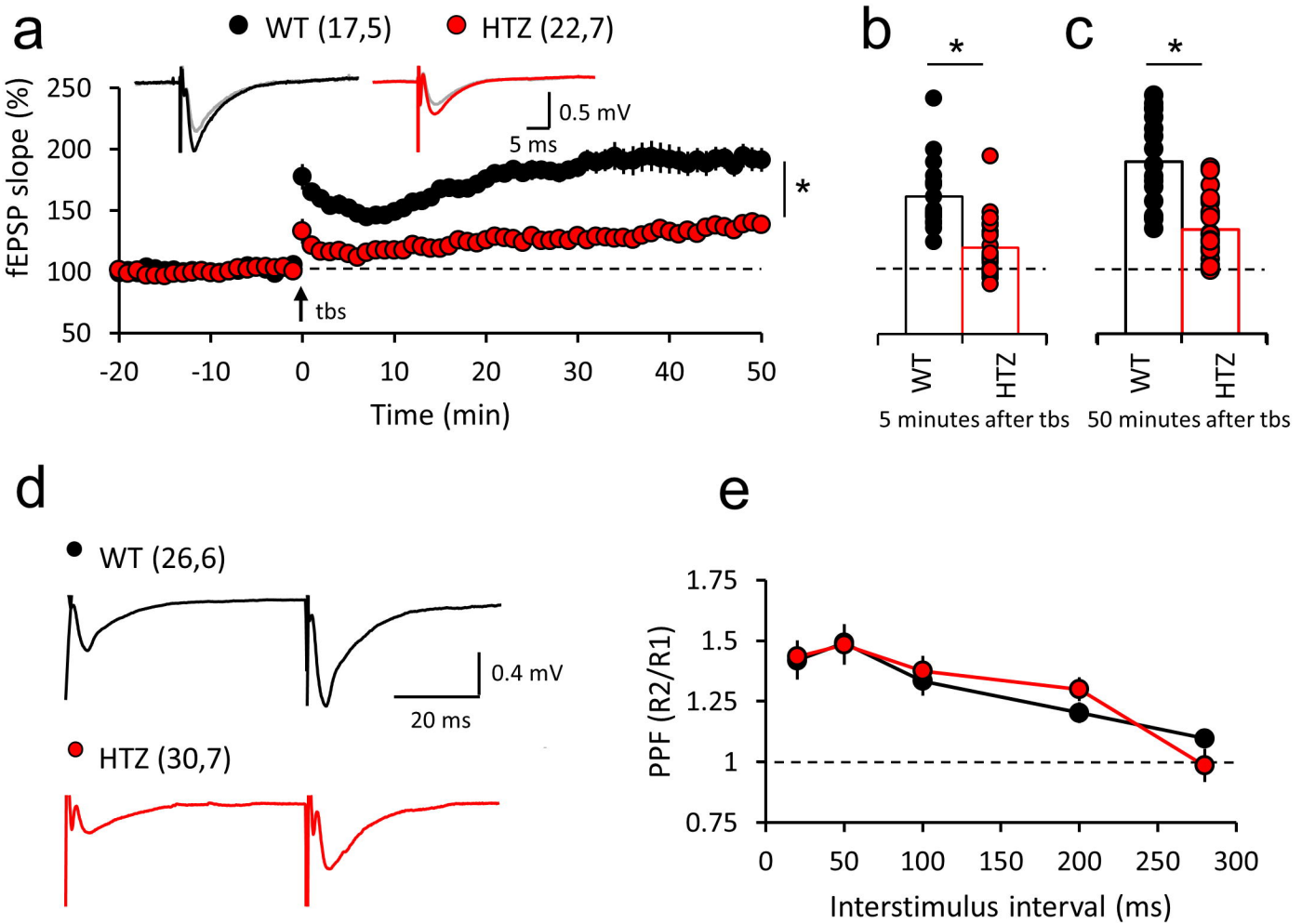
a
WT (17,5)
HTZ (22,7)
fEPSP slope (%)
250
200
150
100
50
0.5 mV
5 ms
*
tbs
-20
-10
0
10
20
30
40
50
Time (min)
b
*
WT
HTZ
5 minutes after tbs
c
*
WT
HTZ
50 minutes after tbs
d
WT (26,6)
0.4 mV
20 ms
HTZ (30,7)
e
PPF (R2/R1)
1.75
1.5
1.25
1
0.75
0
50
100
150
200
250
300
Interstimulus interval (ms)

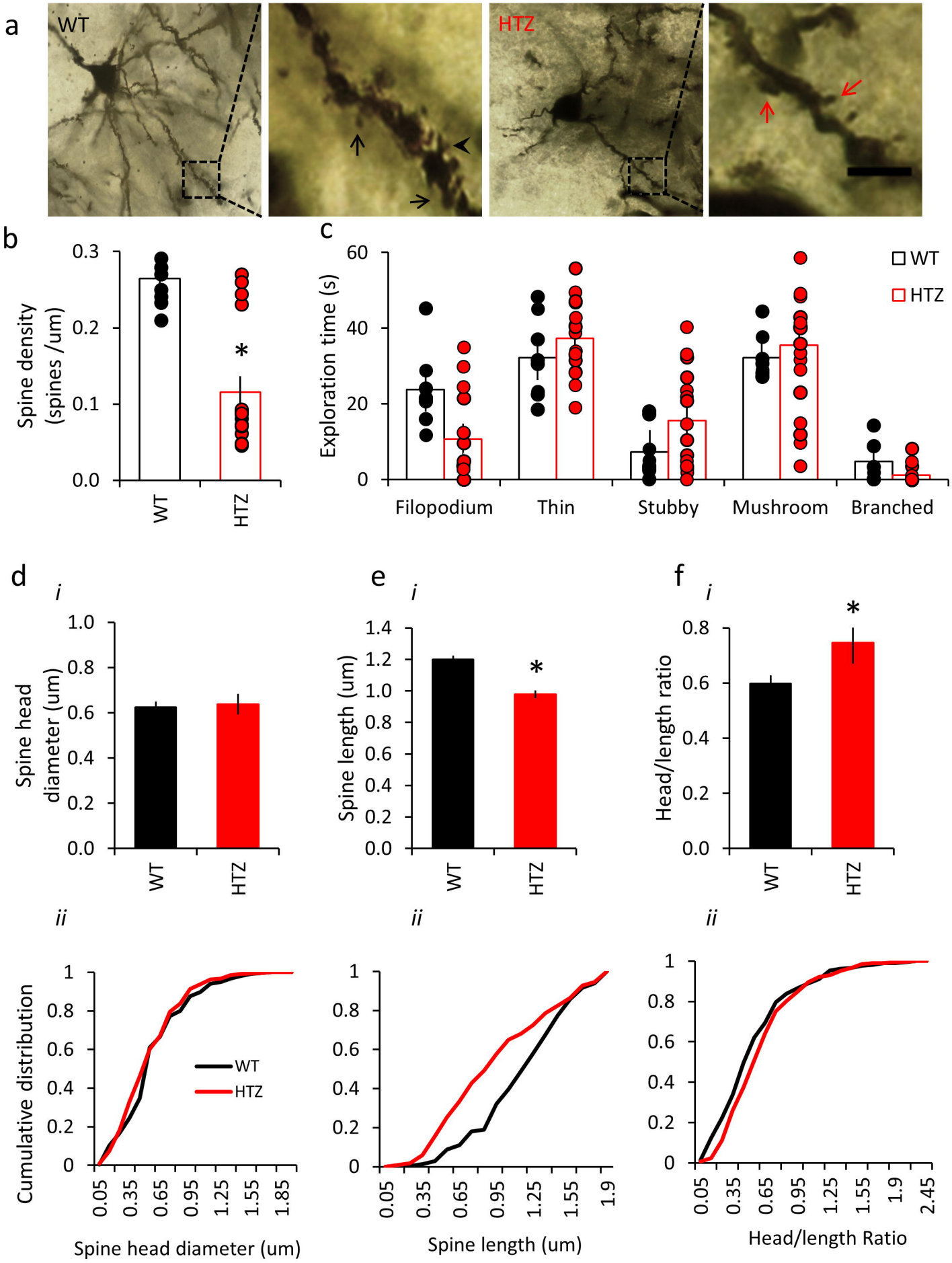
a
WT
HTZ
b
Spine density (spines /um)
0.3
0.2
0.1
0.0
*
WT
HTZ
c
Exploration time (s)
60
40
20
0
WT
HTZ
Filopodium
Thin
Stubby
Mushroom
Branched
d
i
Spine head diameter (um)
1.0
0.8
0.6
0.4
0.2
0.0
WT
HTZ
ii
Cumulative distribution
1
0.8
0.6
0.4
0.2
0
WT
HTZ
0.05
0.35
0.65
0.95
1.25
1.55
1.85
Spine head diameter (um)
e
i
Spine length (um)
1.4
1.2
1.0
0.8
0.6
0.4
0.2
0.0
*
WT
HTZ
ii
1
0.8
0.6
0.4
0.2
0
0.05
0.35
0.65
0.95
1.25
1.55
1.9
Spine length (um)
f
i
Head/length ratio
0.8
0.6
0.4
0.2
0.0
*
WT
HTZ
ii
1
0.8
0.6
0.4
0.2
0
0.05
0.35
0.65
0.95
1.25
1.55
1.9
2.45
Head/length Ratio

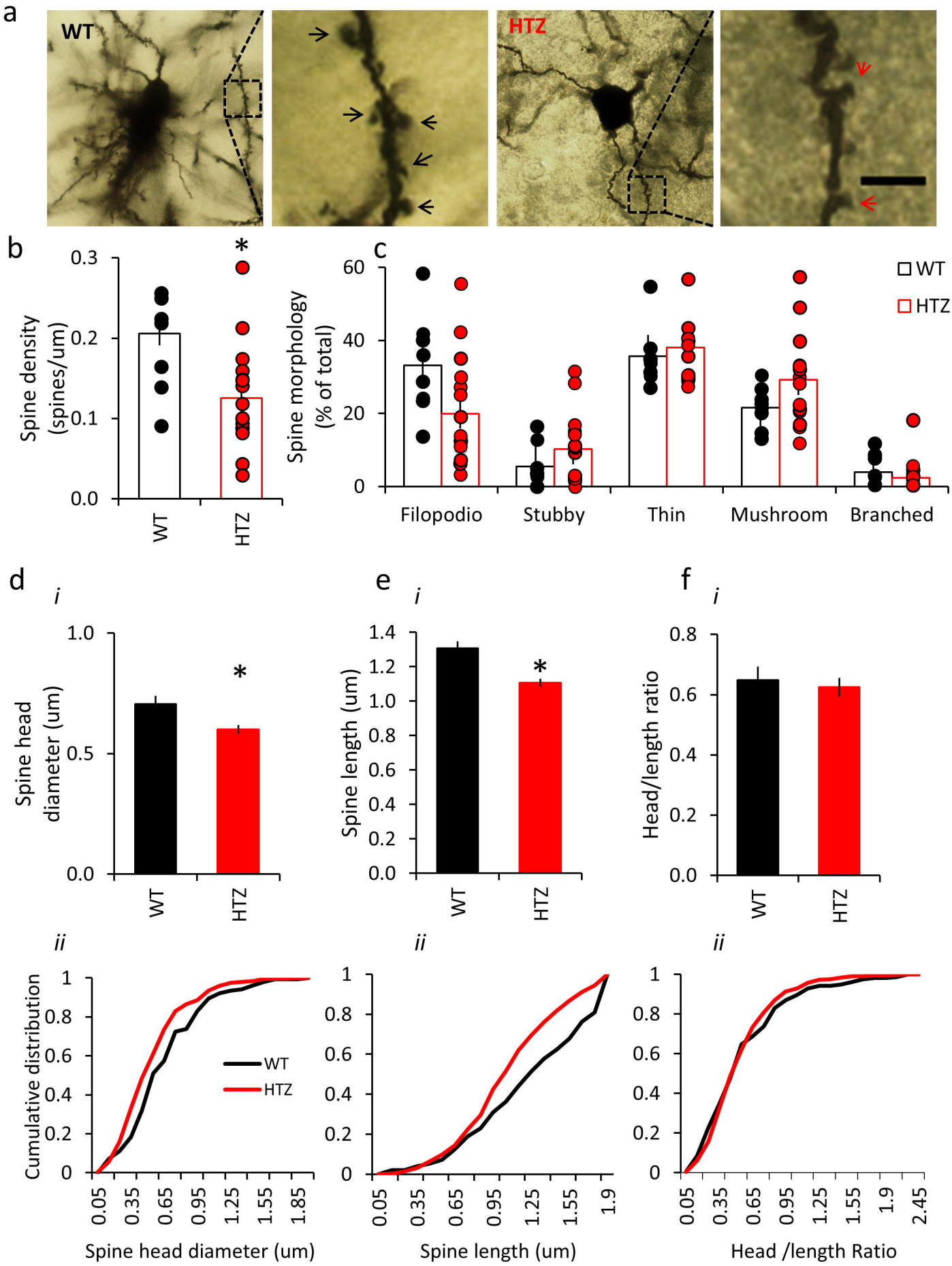
a
WT
HTZ
b
Spine density (spines/um)
0.3
0.2
0.1
0.0
*
WT
HTZ
c
Spine morphology (% of total)
60
40
20
0
WT
HTZ
Filopodio
Stubby
Thin
Mushroom
Branched
d
i
Spine head diameter (um)
1.0
0.5
0.0
*
WT
HTZ
ii
Cumulative distribution
1
0.8
0.6
0.4
0.2
0
WT
HTZ
0.05
0.35
0.65
0.95
1.25
1.55
1.85
Spine head diameter (um)
e
i
Spine length (um)
1.4
1.2
1.0
0.8
0.6
0.4
0.2
0.0
*
WT
HTZ
ii
0.05
0.35
0.65
0.95
1.25
1.55
1.9
Spine length (um)
f
i
Head/length ratio
0.8
0.6
0.4
0.2
0.0
WT
HTZ
ii
0.05
0.35
0.65
0.95
1.25
1.55
1.9
2.45
Head /length Ratio

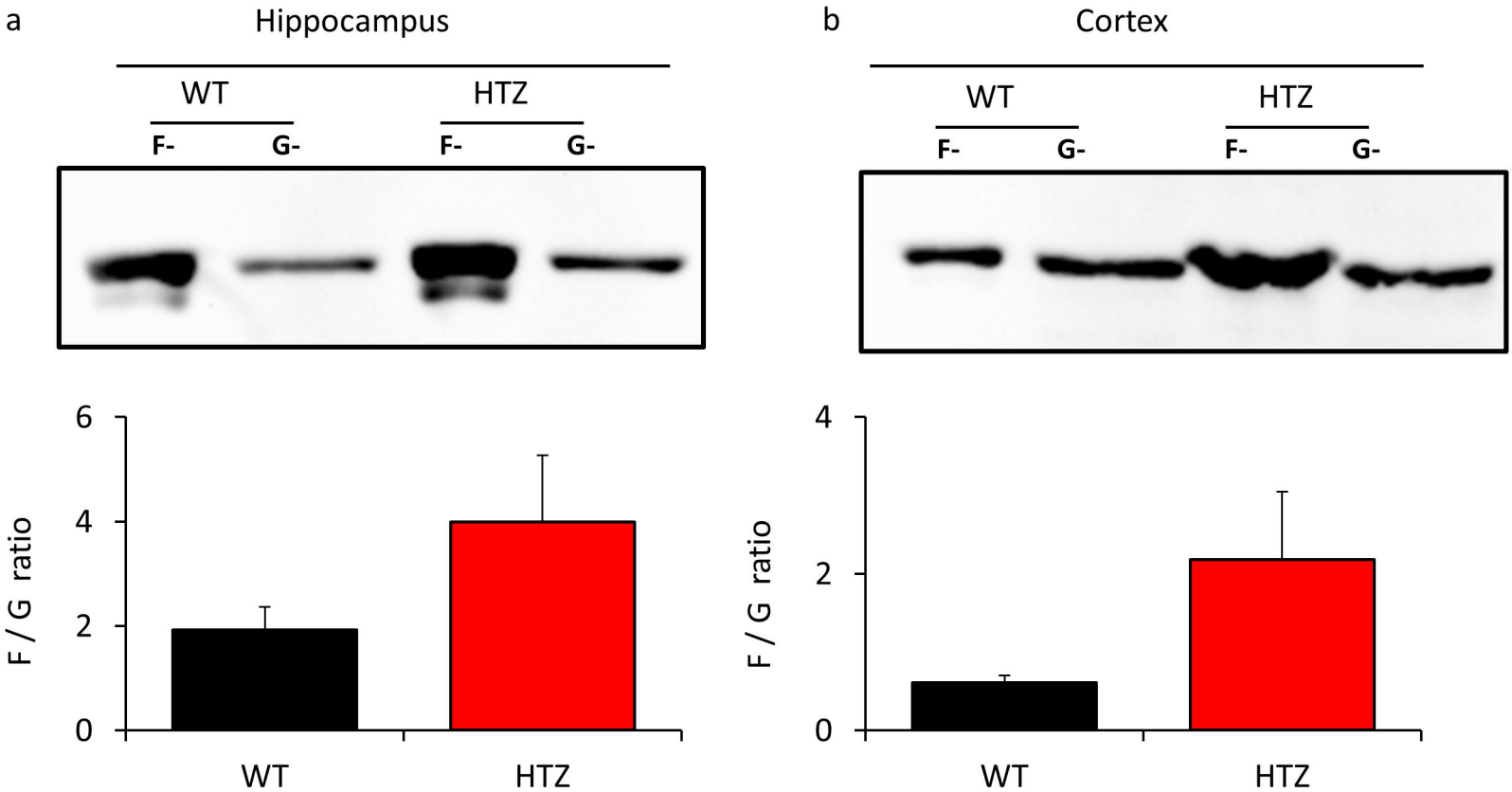
a
Hippocampus
WT
HTZ
F-
G-
F-
G-
6
4
2
0
F / G ratio
WT
HTZ
b
Cortex
WT
HTZ
F-
G-
F-
G-
4
2
0
F / G ratio
WT
HTZ

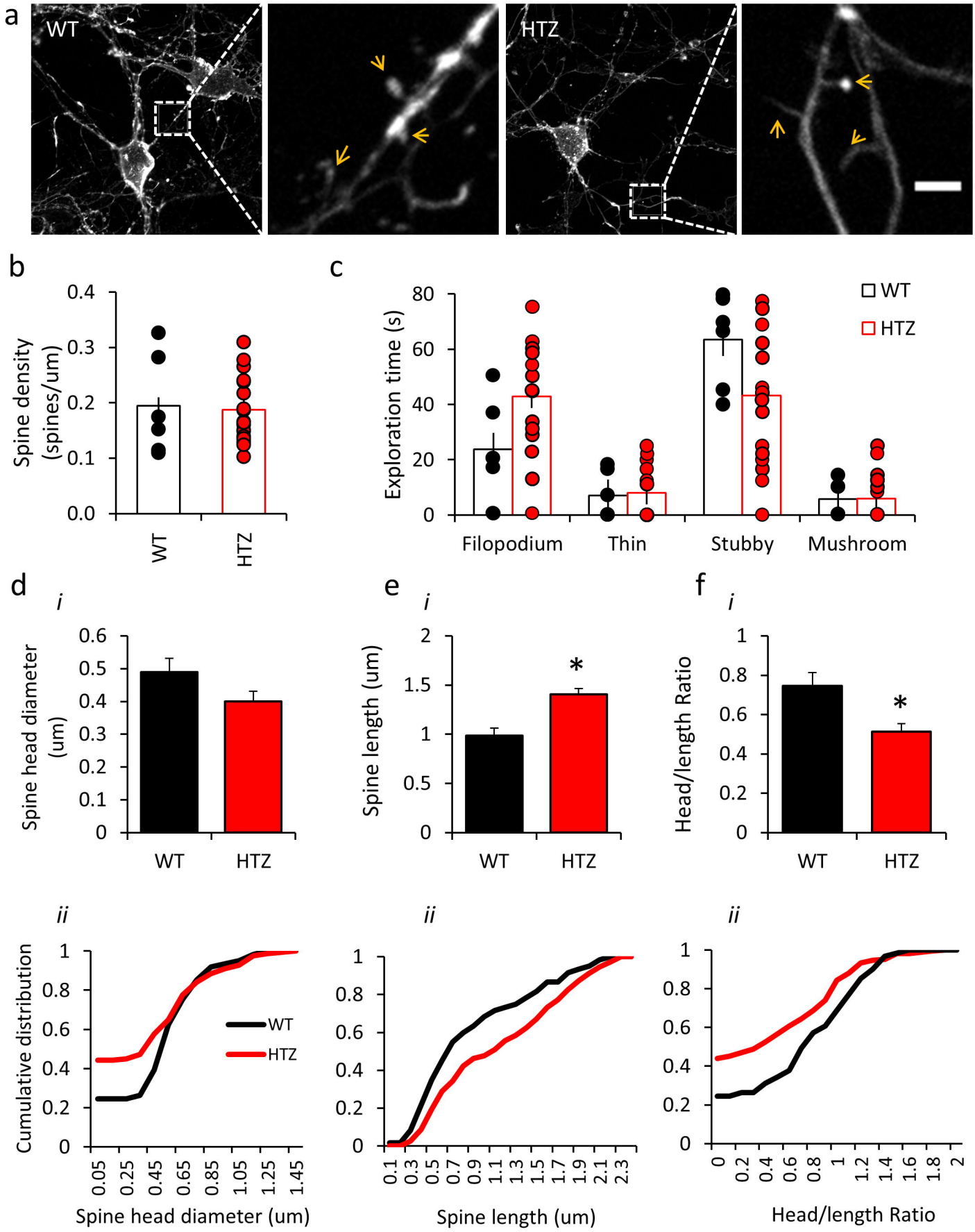
a
WT
HTZ
b
Spine density (spines/um)
0.4
0.3
0.2
0.1
0.0
WT
HTZ
c
Exploration time (s)
80
60
40
20
0
WT
HTZ
Filopodium
Thin
Stubby
Mushroom
d
i
Spine head diameter (um)
0.6
0.5
0.4
0.3
0.2
0.1
0
WT
HTZ
ii
Cumulative distribution
1
0.8
0.6
0.4
0.2
0
WT
HTZ
0.05
0.25
0.45
0.65
0.85
1.05
1.25
1.45
Spine head diameter (um)
e
i
Spine length (um)
2
1.5
1
0.5
0
*
WT
HTZ
ii
1
0.8
0.6
0.4
0.2
0
0.1
0.3
0.5
0.7
0.9
1.1
1.3
1.5
1.7
1.9
2.1
2.3
Spine length (um)
f
i
Head/length Ratio
1
0.8
0.6
0.4
0.2
0
*
WT
HTZ
ii
1
0.8
0.6
0.4
0.2
0
0
0.2
0.4
0.6
0.8
1
1.2
1.4
1.6
1.8
2
Head/length Ratio

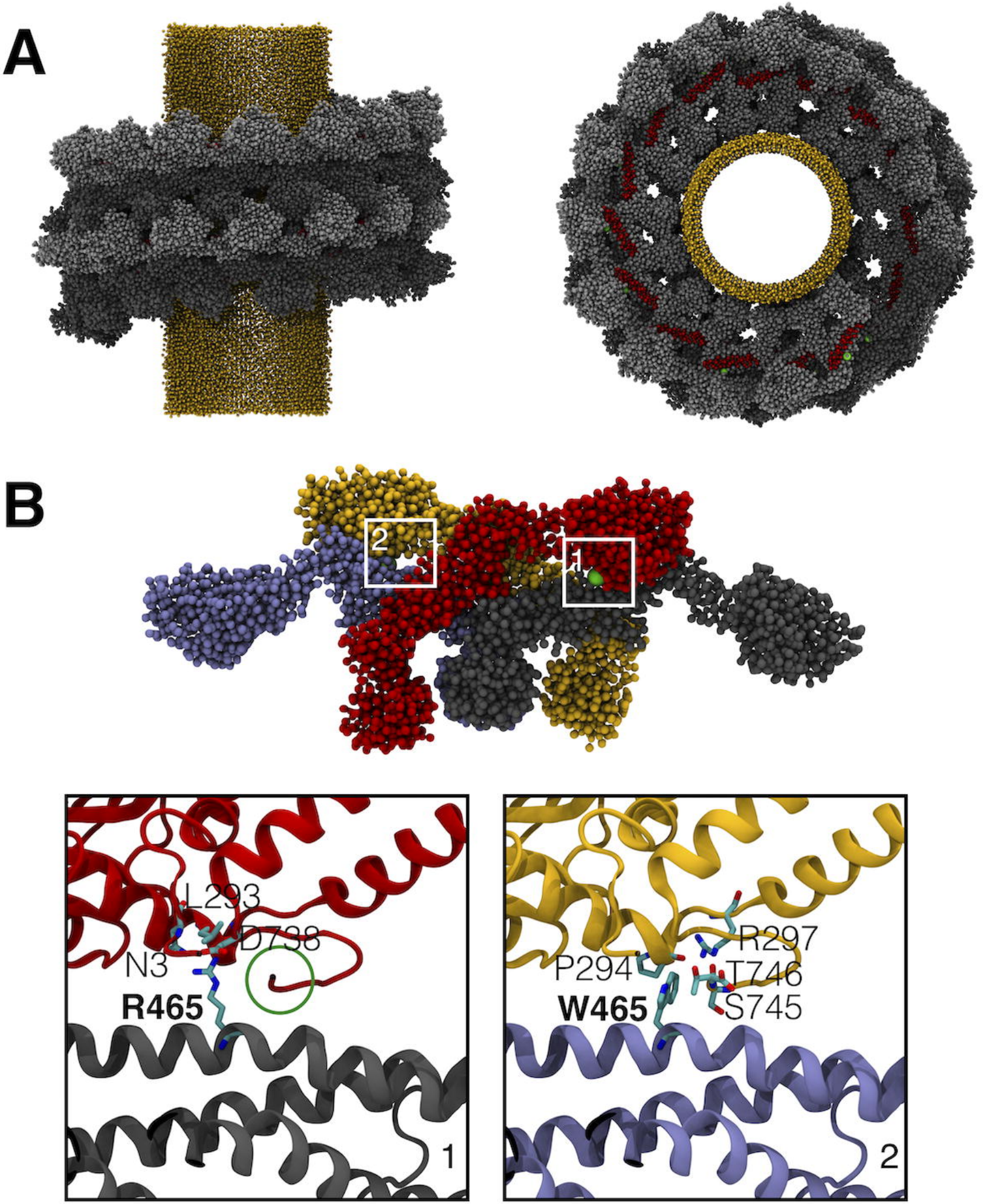
A
B
2
1
L293
D738
N3
R465
1
R297
P294
T746
W465
S745
2